Politecnico di Torino

Modelling of thermal management in metal hydride-based hydrogen storage for stationary applications

Supervisors:

Andrea Lanzini
Francesco Demetrio Minuto
Elena Rozzi

Candidate:

Elisa Maurizi

Abstract

Achieving the greenhouse gas emissions reductions needed to meet commitments under the Paris Agreement and the EU's climate neutrality objective requires a fundamental shift towards clean and sustainable energy systems, while promoting innovation in renewable energy technologies. In the transition towards renewable sources for energy production, hydrogen is an emerging key energy vector, enabling efficient storage and transport of energy. However, due to the intermittent nature of renewable energy sources, reliable and flexible hydrogen storage solutions are required to ensure energy stability.

This study is part of the broader field of innovative technologies for hydrogen storage and transport, as well as its transformation into derivatives and e-fuels. Among the various hydrogen storage technologies, this study focuses on metal hydrides, which store hydrogen through a chemisorption process. This method offers significant advantages over conventional storage techniques, particularly in terms of high volumetric energy density and enhanced safety due to the solid-state containment of hydrogen. However, the absorption of hydrogen in metal hydrides is an exothermic reaction, making effective heat dissipation a critical factor in ensuring optimal performance. The practical implementation of metal hydride storage systems requires addressing these thermal management challenges.

This thesis presents the development of a mathematical model aimed at supporting the scale-up of a hybrid hydrogen storage system. The design of metal hydride storage requires analysis based on its thermophysical properties such as activation/deactivation energy, enthalpy of formation, equilibrium pressure, reaction kinetics and external thermal management system. The model has been designed to be applicable to different metal alloys and boundary conditions. It provides the temperature profiles as a function of the hydrogen flow rate analysing the heat fluxes through the reactor. In particular, the case of a cylindrical reactor placed between an electrolyser and a fuel cell for stationary application has been examined. For the proposed reactor geometry, it has been observed that the hydrogen inlet flow rate must be reduced compared to the maximum allowable rate dictated by reaction kinetics alone, to ensure proper thermal regulation.

The proposed technology represents a promising solution for scalable, efficient, and safe hydrogen storage, with potential applications in stationary civil and industrial energy systems. The findings indicate that while reaction kinetic do not inherently limit the hydrogen absorption

process, effective heat management remains a critical factor in ensuring system efficiency. Further optimization of the tank geometry and operational parameters could enhance performance, making metal hydride-based storage an even more reliable option for future hydrogen energy systems.

List of contents

List of figures

List of tables

1 Introduction

1.1 Towards a sustainable future: Sustainable Development Goals and European strategies

Over the past decades, the United Nations Member States have recognized the importance of a global change towards a more sustainable development and the need for a global action. In 2015, UN Member States adopted "*The 2030 Agenda for Sustainable Development*". It provided a shared blueprint for ending poverty, protecting the planet and tackling inequalities. At its heart there were the 17 *Sustainable Development Goals* (*SDGs*) [Figure 1-1], which still represent an urgent call for action by all countries - developed and developing - in a global partnership. They offer the most practical and effective pathway to tackle the causes of violent conflict, human rights abuses, climate change and environmental degradation and aim to ensure that no one will be left behind. The *SDGs* cover the three dimensions of sustainable development: the economy, social development and the environment. As stated in the aforementioned Agenda, sustainable development everywhere must integrate economic growth, social well-being and environmental protection, with strategies that improve health and education, reduce inequality, and spur economic growth, all while tackling climate change and working to preserve our oceans and forests [1], [2].

Figure 1-1 Sustainable Development Goals [2].

Among these objectives, particular attention is given to *SDG 7* (Affordable and Clean Energy) and *SDG 13* (Climate Action), as they are directly related to the work undertaken in this study. *SDG 7* stresses the transition towards clean and sustainable energy systems, promoting

innovation in renewable energy technologies, improving energy efficiency and ensuring equitable access to modern energy services. Despite improvements and renewable energy growth, at the current pace, by 2030 about 660 million people will still lack access to electricity and close to 2 billion people will still rely on polluting fuels and technologies for cooking. The use of harmful and polluting cooking fuels such as charcoal, wood, agricultural waste and animal dung cause of premature death and serious health issues in many of the poorest regions of the world. Women suffer the worst impacts from the lack of clean cooking. The responsibility of collecting fuel and preparing meals often falls on women. The time spent on these tasks prevents them from fully participating in social, political, and economic activities. It hinders their empowerment and perpetuates cycles of poverty and marginalization, thereby reinforcing social inequalities and gender discrimination [3]. Achieving this goal is crucial for sectors like industry, healthcare and transport, as it provides the basis for sustainable economic and social development [4].

The *Goal 13* focuses on climate action. It aims to fight climate change and its impacts promoting urgent actions at all levels to reduce greenhouse gas emissions. The main objective of this goal is to limit the increase of global temperatures to 1.5°C, as outlined in the *Paris Agreement*. Global warming and related risks are compounded by rising greenhouse gas emissions. The energy sector is responsible for around three-quarters of global greenhouse gas emissions, with fossil fuels as dominant source of energy production worldwide. Climate change is a global challenge that transcends national boundaries. Indeed, communities around the world are suffering from extreme weather phenomena. Extreme temperatures, droughts, floods, wind threats and wildfires affect energy production, infrastructure and power grid operations; rising temperatures drive cooling demand which can cause increase in energy consumption. Shifting energy production to renewable sources, ensuring energy security and increasing energy efficiency, is essential to the achievement of net zero by 2050 [3], [5].

As stated, the effective implementation of the *Sustainable Development Goals* necessitates collaboration with national, regional, and local authorities, along with the active involvement of civil society and the private sector. The European Commission has demonstrated a resolute commitment to the transformation of the EU into a clean, resource-efficient, and competitive economy. The *European Green Deal*, a comprehensive policy initiative, has been devised to achieve these objectives. It aims to ensure zero emissions by 2050, thereby positioning Europe as the first climate-neutral continent globally. The European Commission has adopted the "*Fit for*

55", a package of proposals to transform the EU's climate, energy, transport and taxation policies to reduce net greenhouse gas emissions by at least 55% by 2030 compared to 1990 levels [6], [7].

1.2 The role of hydrogen in the energy transition

In the context of the growing commitment to climate neutrality, hydrogen is an emerging key component thanks to its properties. Hydrogen is considered one of the most versatile solutions to decarbonise sectors where emissions are challenging to reduce. Energy-intensive sectors such as heavy industry, shipping, aviation, etc. are difficult to electrify directly, and hydrogen has been demonstrated to offer a variety of pathways that have the potential to facilitate a transition to more sustainable operations [8].

Hydrogen is the most abundant element in the universe but rarely available in the free and molecular state (H_2). It constitutes a minor percentage of the total energy consumption in the EU and the rest of the world. Presently, less than 2% of European energy consumption is attributed to hydrogen, which is predominantly used in the production of chemicals such as plastics and fertilisers. Hydrogen requires a primary energy source for production, and the choice of process and energy source determine the environmental impact and pollution levels of the final product. Notably, most of the hydrogen is derived from natural gas, a process that results in substantial CO_2 emissions. The primary challenge, therefore, is to decarbonise hydrogen production. Fossil-based hydrogen is called *grey hydrogen* and is by far the most common type currently used. In addition, low-carbon hydrogen, categorised as *blue hydrogen*, is derived from natural gas. Nevertheless, the CO_2 emissions during its production are captured and sequestered, thereby reducing its environmental impact. The production of low-carbon gases does not utilise renewable energy sources; however, these gases generate at least 70% fewer greenhouse gas emissions than fossil natural gas over the entire lifecycle [9]. While low-CO_2 hydrogen can serve as a crucial transitional fuel, replacing grey hydrogen, the most environmentally friendly option is renewable hydrogen, also referred to as *green hydrogen*. The latter is produced from renewable energy sources, such as wind and solar power, using an electrolyser. This method of production is almost entirely emission-free, renders green hydrogen the most attractive option [8].

Green Hydrogen is particularly appealing for applications in the energy sector as an energy vector or as an energy storage, and it can replace fossil gas in the gas market [10]. In the field of heavy transportation, hydrogen is emerging as a promising alternative fuel. The transport sector is responsible for almost 25% of greenhouse gas emission in the EU. The integration of hydrogen fuel

cells in long-distance vehicles offers significant advantages in terms of rapid refuelling times, given the constraints and costs associated with contemporary battery technologies [11], [12]. Thanks to its high energy content, hydrogen has been identified as playing a pivotal role also in high energy intensive industrial processes. Such processes include the production of steel, concrete and fertiliser, which have historically relied on fossil fuels such as coal and natural gas. By replacing these energy sources, industries can significantly reduce their greenhouse gas emissions while maintaining operational efficiency.

As previously stated, the transition to renewable energy sources, such as solar and wind power, is imperative for the establishment of a sustainable and low-carbon energy system. The growing deployment of renewable energy sources goes hand in hand with an electricity sector that is increasingly dominated by renewable energy production. It has been anticipated that clean energy sources will achieve unprecedented levels of success in the global power generation sector during the 2025-2027 forecast period [Figure 1-2*Errore. L'origine riferimento non è stata trovata.*]. Low-emission sources, encompassing renewable energy and nuclear power, are projected to satisfy the entire global demand for energy growth up to the year 2027. Solar photovoltaic (PV) energy is poised to become the second largest low-emissions source of electricity generation worldwide by the year 2027, following hydropower. Furthermore, it is anticipated that renewable sources, when considered collectively, will exceed coal-fired generation by 2025, marking a significant shift in the global energy landscape. This transition will also result in a decline in coal's share below 33%, a milestone that has not been observed in the past century [13].
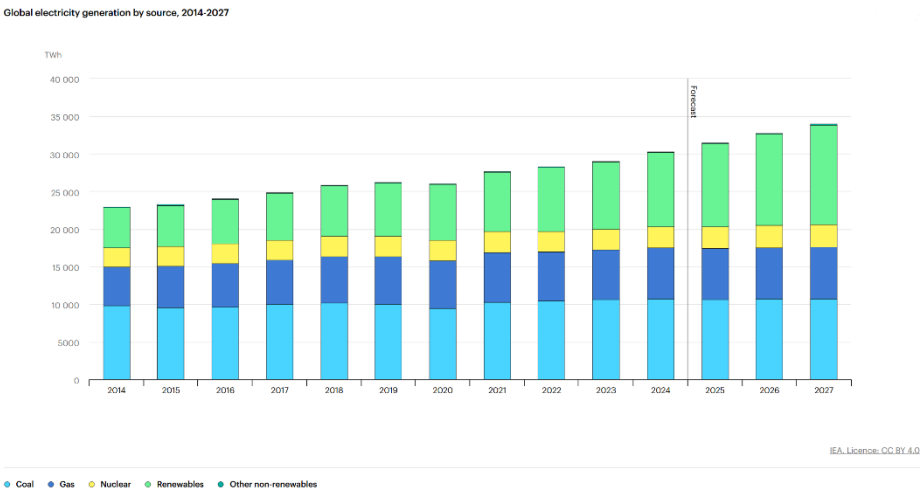
Figure 1-2 Global electricity generation by source, 2014-2027, IEA - Electricity 2025 [12].

As the share of renewable energy sources in the electricity generation mix rises, understanding periods with reduced wind and solar PV generation due to weather conditions becomes critical. These energy sources are inherently intermittent and unpredictable, which poses a substantial challenge to energy security and grid stability [13]. The availability of solar and wind energy is subject to fluctuations depending on weather conditions, time of day and seasonal variations. This variability can lead to periods of excess generation, when energy supply exceeds demand, and times of scarcity, when energy output is insufficient to meet demand. Temporary periods with reduced wind and solar PV generation may put additional strain on the power system, especially if they occur during periods of high electricity demand, such as during colder winter seasons with increased heating demand, or hotter summers with higher cooling load [13]. To guarantee a continuous energy supply, the entire energy systems must become more flexible to accommodate these natural fluctuations. It is needed to possess sufficient dispatchable capacity and long-duration storage, in addition to a range of flexibility options to enhance electricity security. This flexibility can be achieved through various means, including advanced grid management, energy storage solutions, demand-side response and sector coupling. Significant investments are being directed towards the development of integrated energy infrastructures, with the aim of facilitating interaction between electricity grids and gas networks. By coupling the power sector with other sectors, such as the heating and transport sectors, surplus renewable energy can be used more effectively. In this specific context, hydrogen has a relevant role in power-to-X technologies. The electricity surplus produced by renewable sources can be converted into other forms of energy, for example in hydrogen in the case of power-to-hydrogen technologies. Then the hydrogen produced can be stored and reconverted when energy demand is high or can be used in different sectors, ensuring a reliable and secure energy supply while maximizing the potential of renewable sources. In this sense, hydrogen serves as a form of "long-duration battery", helping stabilize the grid and ensuring a continuous energy supply, even during periods of low renewable generation.

2 Hydrogen storage

Hydrogen has garnered significant attention for its considerable potential across a range of sectors, including transportation, power generation and industry. As a key sustainable alternative to fossil fuels, hydrogen produced via water electrolysis can be efficiently converted into thermal, mechanical and electrical energy. Green hydrogen can be directly utilised as feedstock, injected as fuel in stationary and automotive fuel cells, injected into the natural gas grid, converted into synthetic fuels like methane, or stored for future use [Figure 2-1]Figure 2-1 Green hydrogen pathways. In light of the intermittent nature of renewable energy sources, the development of effective hydrogen storage solutions is essential to ensure the balance of supply and demand, contributing to the stability and reliability of the energy system [14].

There are two main issues that prevent the generalised use of hydrogen as an efficient fuel, and thus the energy transition towards a compelling fossil-free solution. Firstly, hydrogen is an energy vector, energy is needed to produce it. Secondly, despite exhibiting a high energy content (LHV= 120 MJ/kg), hydrogen has a density of 0.089 kg/m^3 at 0 °C and 1 atm. Following production and prior to use, hydrogen is packaged, distributed, stored and delivered. The most complex issues to be resolved are those related especially to the latter two steps [14], [15].

Hydrogen storage is therefore a key challenge. To date, H_2 storage is often achieved by compressing H_2 and this remains the most widespread method due to the maturity and simplicity of the technology [14], [16]. However, H_2 storage can also be implemented by liquefaction or as solid-state storage, mainly in the form of metal hydrides and advanced materials [16]. The US Department of Energy (DOE) has established specific performance criteria for hydrogen storage technologies, particularly for applications in transportation and stationary systems. Key targets include a gravimetric hydrogen density of at least 5.5 wt.%, with a long-term goal of 6.5 wt.%, and a volumetric density greater than 40 kg/m^3 to ensure practical and efficient storage solutions [17]. These standards guide ongoing research and development to improve storage efficiency, safety and cost effectiveness. This section aims to provide a brief overview of the state of the art of hydrogen storage technologies by analysing their main characteristics, operating principles and potentially achievable performance. For each technology, its current advantages and limitations are highlighted and its applicability in different energy network configurations is assessed in terms of efficiency, safety, cost and infrastructure requirements.
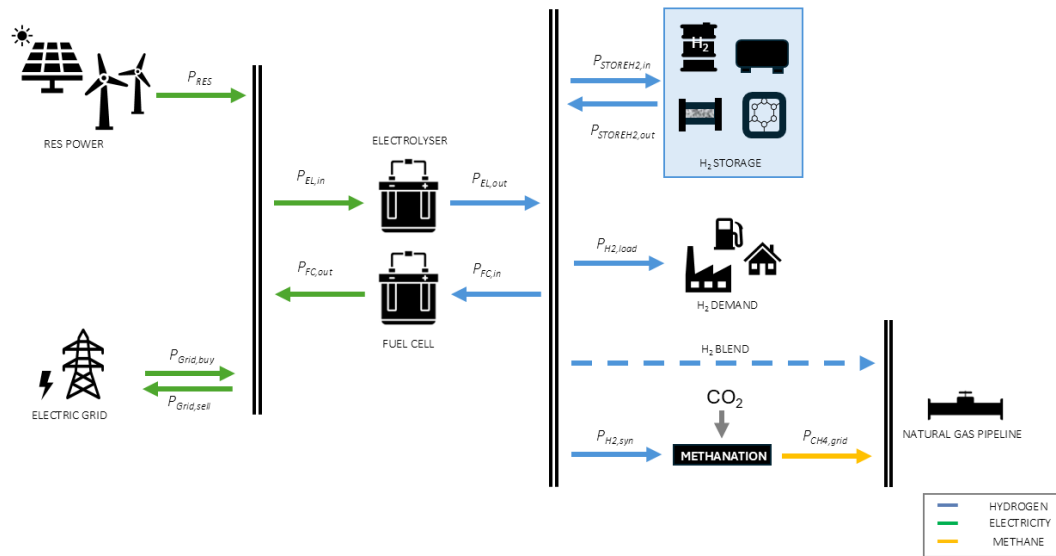
Figure 2-1 Green hydrogen pathways.

Mechanical compressors represent the most prevalent technology in contemporary use, operating on the principle of direct conversion of mechanical energy into gas energy. Among the various typologies, positive displacement devices are particularly utilised for hydrogen compression, involving the reduction of the confined volume within which hydrogen is contained, through the utilisation of a piston [14]. Hydrogen can be stored at high pressures, typically between 350 and 700 bar. The primary advantages of mechanical compressors lie in their technological readiness, widespread availability and maturity. They are commonly implemented in fuel cell vehicles and hydrogen refuelling stations. However, a significant drawback is the high energy consumption required for compression. Additionally, the use of lubricating oils for the reciprocal movement of mechanical components poses a risk of hydrogen contamination, necessitating the use of oil-free designs. These compressors require strong, lightweight materials capable of withstanding extreme pressures. Their complex structure, consisting of multiple moving parts, increases both manufacturing costs and maintenance challenges. Furthermore, the interaction between hydrogen and metal surfaces can lead to embrittlement phenomena, potentially compromising the structural integrity of the compressor components over time [18]. Safety remains a critical concern due to the high pressures involved, which are necessary to enhance volumetric energy density but also increase the risk of leaks.

A divergent approach to hydrogen storage entails the utilisation of liquid storage methodologies. Liquefaction of hydrogen requires cooling it to cryogenic temperatures (-253 °C) to achieve higher

energy density compared to compressed gas storage. This technology is suitable for long-distance transport and large-scale storage. It is used in aerospace applications and hydrogen refuelling stations. The cost associated with liquefaction is high, almost the 30% of the hydrogen energy content is lost in the process [16]. The low temperatures involved necessitate effective thermal management, which in turn requires sophisticated insulation and handling infrastructure. Cryo-compression rely on the achievement of high pressures at very low temperatures. This solution allows storing 2-3 times more fuel than using conventional ambient-temperature compressed vessels. Whereas a pressure of 75 MPa is indeed necessary for storing 4.1 kg of hydrogen in 100 L at room temperature, a pressure of 15 MPa is required to compress the same amount when the temperature is decreased to 77K [19], [20]. Nevertheless, the low temperatures involved result in higher system complexity and the high energy cost is a strict limitation.

Solid-state storage involves the chemisorption or physisorption of hydrogen in materials such as metal hydrides and porous materials. Physisorption hydrogen storage relies on the ability of hydrogen to bind weakly to the surface of high porous solids, such as carbonaceous materials or metal-organic frameworks (MOFs). The interaction energies involved are low, typically ranging from 0.01 to 0.1 eV, which results in the absence of chemical bonds between hydrogen molecules and the solid substrate [21]. Hydrogen interacts with the solid bed surface through weak Van der Waals forces, forming a monolayer on the adsorbent surface, thereby classifying it as a physisorption process. The effectiveness of this method is significantly influenced by the properties of the adsorbent materials and operating conditions. Several classes of porous materials have been investigated for hydrogen storage through physisorption like Activated Carbons (ACs), Metal-Organic Frameworks (MOFs), Covalent Organic Frameworks (COFs) and Zeolites. The adsorbent material performance is influenced by factors such as pore size and surface. The structure can be engineered to obtain higher surface areas and optimal pore sizes, thereby enhancing hydrogen uptake and providing more adsorption sites. However, due to the weak interactions involved, physisorption-based hydrogen storage requires low operating temperatures to achieve significant hydrogen uptake. Disadvantages include the low thermal conductivity of most adsorbents which makes thermal management difficult, limiting their practical applications. In addition, porous materials may exhibit structural instability or degradation under operating conditions, affecting their performance over time and causing a decreasing stability over cycles. In order to achieve the requisite standards for commercial

8

applications, further refinements are necessary. They still do not compete with metal hydrides in terms of kg H_2/kg material. Metal hydrides absorb hydrogen through a chemisorption process, they have the potential to store hydrogen at higher energy densities than compressed and liquefied hydrogen, while minimizing the safety risk associated with high pressure systems [16], [22]. Metal hydrides are considered to be among the most promising materials for hydrogen storage. This is due to their ability to reversibly absorb and release hydrogen when required, at moderate pressures and temperatures. This makes them potentially suitable for integration into stationary and mobile hydrogen storage applications [23]. However, the absorption of hydrogen in metal hydrides is an exothermic reaction, making effective heat dissipation a critical factor in ensuring optimal performance. The practical implementation of metal hydride storage systems requires addressing these thermal management challenges. A further significant limitation of metal hydrides is their vulnerability to material degradation over multiple charge and discharge cycles, which can impact their long-term efficiency and durability. Additionally, the limited availability and high cost of certain metal hydride materials impose economic constraints on large-scale adoption. Despite these challenges, metal hydrides remain a highly researched field, with ongoing advancements focused on enhancing their hydrogen storage capacity, improving reaction kinetics and increasing overall stability. An overview analysis of their absorption mechanisms, material properties, performance, and application in hydrogen storage will be provided in the following chapter.

3 Hydrogen chemisorption: metal hydrides

Various metals present in the periodic table have the capacity to store hydrogen in the form of hydrides. This process occurs through the direct dissociative chemisorption of H_2 gas following the reaction:

$$M + \frac{x}{2}H_2 \leftrightarrow MH_x$$
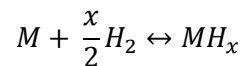
where M is the metal, x is the hydrogen concentration and MH is the resulting metal hydride. The process of hydrogen absorption is exothermic, resulting in the release of heat. Conversely, desorption is endothermic, necessitating the input of heat. The equilibrium between these two processes is governed by the pressure-composition-temperature (PCT) properties, which describe how the hydrogen content in the metal changes as a function of pressure and temperature. The behaviour is commonly expressed in the isothermal P-C hysteresis loop. The system exhibits distinct plateau pressures and temperatures, which are characteristic of the individual materials under consideration. A generalized form of isothermal P-C is shown in Figure 3-1 to elucidate the mathematical and numerical definitions of hysteresis, plateau slope and H-capacity [24].
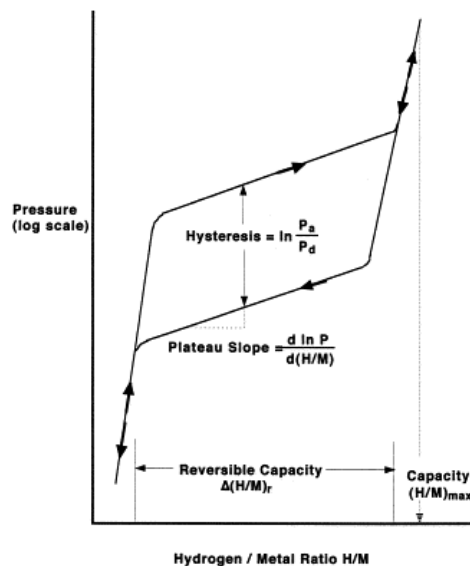
Figure 3-1 Schematic isothermal pressure–composition hysteresis loop [24].

The first key parameters when comparing different storage technologies are usually the gravimetric storage capacity and volumetric energy density. For metal hydrides the gravimetric capacity can be calculated as the quotient of the maximum absorbed hydrogen mass and the

mass of the hydride material and is expressed as weight percent (wt.%). The volumetric energy density is typically specified as:

$$v_{ed} = \frac{m_{H_2} \cdot LHV_{H_2}}{V_{MH}} \qquad (1)$$

Where m_{H_2} is the maximum absorbed hydrogen mass, LHV_{H_2} the lower heating value of hydrogen (120 MJ/kg) and V_{MH} the volume of the hydride material [22].

Thermodynamics dictate the PCT curves. At a given temperature, the equilibrium hydrogen pressure, denoted as the plateau pressure, remains constant within a certain range of hydrogen concentrations. The length and the slope of these plateau regions are critical in defining the material's suitability for storage applications. To determine the operating ranges for pressure and temperature and to compare the thermodynamics of different hydride van't Hoff plots are used [Figure 3-2]. The curves in the Van't Hoff plot can be described with the following equation:

$$ln\left(\frac{P_{eq}}{P_0}\right) = -\frac{\Delta H}{R\,T} + \frac{\Delta S}{R} \qquad (2)$$

Where P_{eq} is the equilibrium plateau pressure, ΔH is the enthalpy of formation of the hydride, ΔS is the entropy, T is the absolute temperature and R is the gas constant [16], [22], [24], [25]. These plots express the natural logarithm of the equilibrium pressure as a function of the inverse temperature. ΔH and ΔS are negative, indicating that the hydriding reaction is an exothermic and the dehydriding reaction is endothermic. The values of both parameters are dictated by the material employed in the reaction. The value of reaction entropy is predominantly influenced by the entropy change of gaseous hydrogen during the reaction; consequently, the entropy values of most metal hydrides are found to be within a comparable range [16], [22], [26]. The reaction enthalpy is represented by the slope of the van't Hoff plot and exhibits significant variation between low- and high-temperature hydrides. Low-temperature hydrides possess lower reaction enthalpies and are capable of functioning at ambient or near-ambient conditions. Consequently, methods for reducing the reaction enthalpy, such as elemental addition or substitution, are advantageous [27]. The enthalpy of formation is a critical parameter that governs the operating temperature and pressure of hydrogen storage materials. It is closely related to the strength of the M–H bond [24]. The term ΔH directly influences the heat released or absorbed during the absorption and desorption cycles. Its knowledge is of particular importance for the thermal management, with the aim of ensuring efficient heat regulation and enhancing overall system efficiency. As illustrated in Figure 3-2, P_{eq} is the resulting equilibrium pressure in the middle of the

plateau of a PCI curve. For the absorption reaction to occur, the pressure of the gaseous hydrogen must be higher than the equilibrium pressure at a given temperature. Conversely, during desorption the hydrogen pressure is lower than the equilibrium pressure. According to Equation (2), an increase in temperature leads to an increase in the equilibrium pressure. Since the absorption reaction is exothermal, the released heat leads to a temperature increase, which in turn leads to a great increase in the required pressure level of the in-flowing gaseous hydrogen. Without of a suitable thermal management system, the reaction inhibits itself, resulting in long filling times [22].
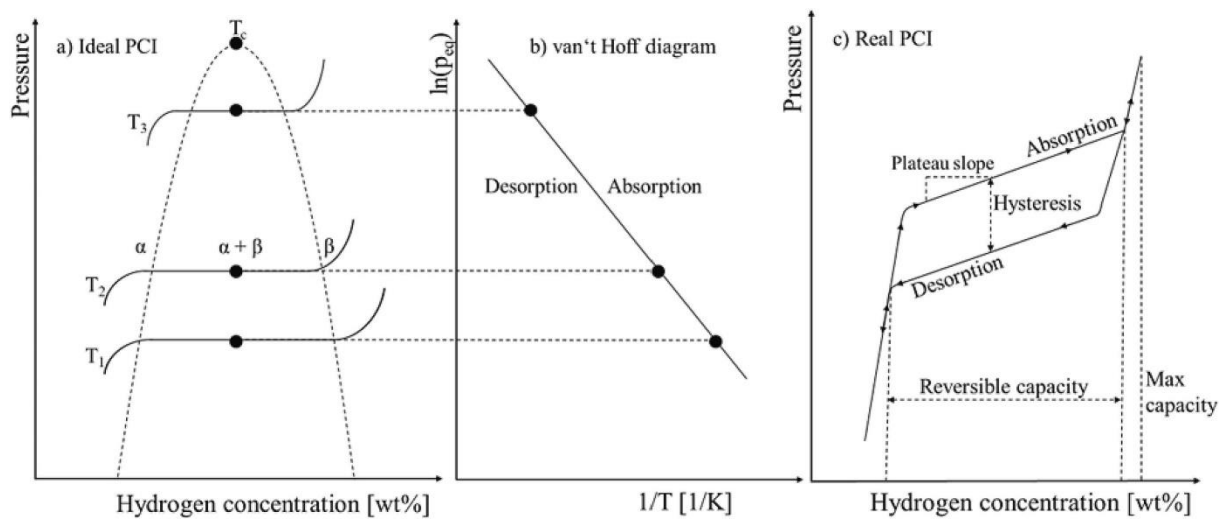
Figure 3-2 a) Ideal PCI at different temperatures with the corresponding b) Van't Hoff plot and c) real PCI with hysteresis and plateau slope [22].

Hydrogen is a highly reactive element and has been shown to form hydrides and solid solutions with many metals. However, individual elements are usually not suitable as practical hydrogen storage materials because of their poor hydrogen storage capacity or the need of high temperatures/pressures for the uptake/release of H2 [16]. As illustrated by the van't Hoff lines of Figure 3-3, the PCT properties for elemental hydrides are not very convenient relative to the 1–10 atm, 0–100 °C range. In order to satisfy the requirements of practical application, the alloys are engineered to achieve the necessary properties. In particular, alloying methods combine strong hydride forming elements A with weak hydriding elements B to have desired intermediate thermodynamic affinities for hydrogen. A "family-tree" of hydriding material is illustrated in Figure 3-4. The focus is primarily on intermetallic compounds due to their ability to operate near ambient conditions. In these compounds, hydrogen is typically bound in interstitial sites causing minor distortions to the generally stable hydrogen-free alloy structures. Intermetallic compounds

can adopt a range of structures, such as AB, AB2, AB5, and others. The detailed analysis of these different compounds is beyond the scope of this study. It should be noted that there is no ideal alloy and the most suitable one must be chosen based on the specific application requirements, comparing all the different properties [24].
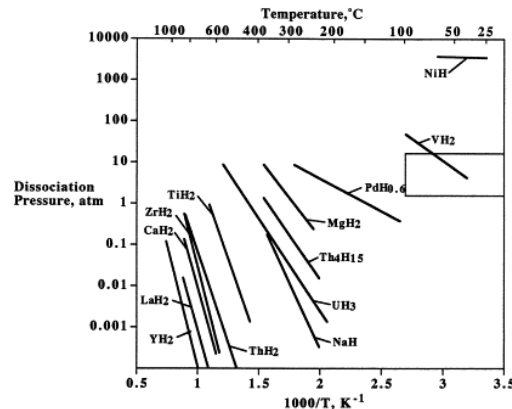
Figure 3-3 Van't Hoff lines (desorption) for elemental hydrides. Box indicates 1–10 atm, 0–100 °C ranges [24].
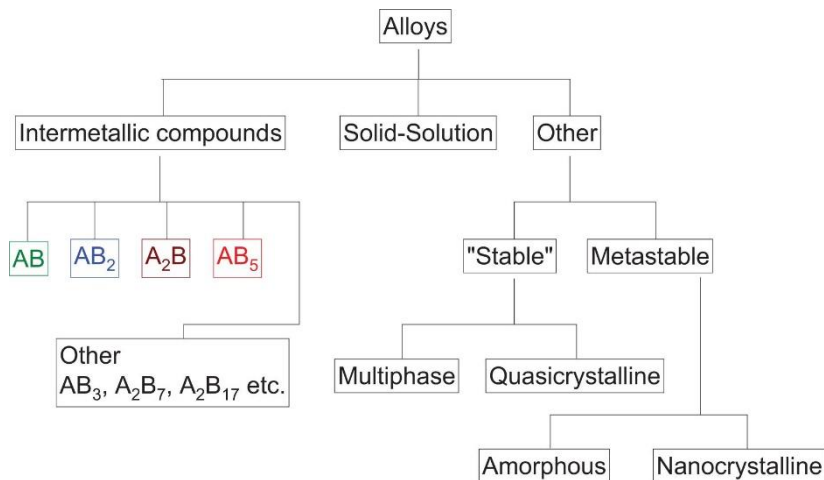
Figure 3-4 Family tree of metal hydrides [16], [24].

Several other important parameters should also be considered when selecting suitable hydride materials. These include the ease of activation of the hydride material for hydrogen uptake/release, the decrepitation phenomenon, its H_2 uptake/release kinetics, its sensitivity to gas impurities, the H_2 hysteresis effects, the cyclic stability as well the safety and the associated costs.

The activation is the process by which a metal is hydride for the first time. This procedure brings it up to the maximum hydrogen capacity and optimize the absorption/desorption kinetics. The ease

with which hydrogen penetrates the metal during the initial stage is largely influenced by the surface structure and barriers like oxide films. Once the initial absorption occurs, a second activation stage takes place, involving the internal cracking of the metal particles, which increases the available surface area for further hydrogen absorption.

Decrepitation is defined as the process by which the material grain is reduced into powder. This phenomenon is the result of a combination of factors: the occurrence of volume changes during the process of hydride formation and the inherent brittleness of hydride alloys. A primary concern with decrepitation is that it further impairs the already limited heat transfer properties, thereby posing a significant challenge for thermal management. Additionally, fine metal hydride particles generated by decrepitation can be transported by hydrogen flow due to drag forces. This phenomenon can negatively impact reactor performance, potentially causing blockages in valves, manifolds, and other critical components.

The kinetics of hydrogen absorption and desorption in metal hydrides can vary significantly among different alloys. Many room-temperature hydrides demonstrate excellent intrinsic kinetics, meaning that the hydrogen absorption/desorption process at the material level occurs with relatively low energy barriers. At the macroscopic scale, the initial hydrogen pressure and temperature often determine the rate-limiting steps, which are frequently governed by heat transfer constraints. At given temperature and pressure conditions, the absorption and release rates are dictated by the alloy's intrinsic properties. The metal–hydrogen interactions can be quantified by the Arrhenius equation:

$$k(T) = A \, e^{\frac{-E_a}{RT}} \quad (3)$$

Where k(T) is the rate constant, E_a is the activation energy and A is the pre-exponential factor.

The resistance of metal hydrides to gaseous impurities is a critical property, since exposure to contaminants can lead to various forms of degradation. Among these, poisoning results in a rapid loss of hydrogen storage capacity, while retardation leads to a decline in reaction kinetics. Reaction damage occurs when the alloy undergoes gradual corrosion, leading to irreversible structural deterioration. Lastly, innocuous damage manifests as pseudo-kinetic limitations caused by inert gas blanketing or interparticle gas diffusion.

Cyclic stability is a critical property, as it influences the longevity and performance of metal hydrides over repeated cycles. Alloys and intermetallic compounds may be susceptible to

disproportionation, where the alloy breaks down to form stable, non-reversible hydrides, resulting in a loss of reversible hydrogen storage capacity. Even if very pure hydrogen is used.

Safety considerations are made in terms of tendency for a hydride powders to burn and of toxicity risks from accidental ingestion or inhalation.

Finally, cost is a crucial factor in assessing the economic feasibility of a metal hydride storage system. However, considering only the cost of raw materials provides an incomplete perspective. The overall production cost of an alloy can increase significantly due to various factors, including melting and annealing processes, metallurgical complexities, and the precision required in tailoring its properties. A comprehensive economic evaluation extends beyond these considerations and falls outside the scope of this study, necessitating further analysis for a complete assessment of the cost-effectiveness of metal hydride-based hydrogen storage systems [16], [24].

Research continues to focus on improving the properties of metal hydride alloys through the modification of alloy compositions and surface treatments [27].

Metal hydride storage systems boast a high degree of versatility, with applications in both stationary and mobile energy storage. The challenge lies in selecting the most appropriate metal hydrides to meet the specific requirements of each use case. These materials serve a broad range of functions, ranging from hydrogen storage in various mobile and stationary applications to compression, purification, (isotope) separation, thermal storage as well as heat pumps [23]. Focusing on stationary application, the main advantage of hydrogen storage in these applications are the high volumetric energy density and lower operating pressure compared to gaseous hydrogen storage. In Power-to-Power (P2P) systems the metal hydride tank is coupled to an electrolyser upstream and a fuel cell or H_2 internal combustion engine downstream. The typical H_2 outlet pressures of PEM-electrolysers are around 30 bar [28], making it high enough to avoid the need of a compressor for the tank refuelling. The required inlet pressure of the anode subsystem of a PEM fuel cell is in the 3 –5 bar range [29], which is an achievable pressure level during desorption from the metal hydride storage. Further advantages include the increased safety, thanks to the lower operating pressure, and the decreased maintenance requirements. Furthermore, by avoiding the need for components able to resist high-pressures, the system cost can be decreased. The high volumetric energy density as well as good scalability make the MH storage suitable for small- to large-scale energy storage. Since no losses of hydrogen occur during

storing, these systems are suitable for mid- to long-term storage. The above requirements and advantages of MH apply to applications such as households/residential areas, off-grid systems, back-up systems and large-scale seasonal storage [22]. However, each of the listed applications presents additional challenges that are out of the scope of this study.

4 Methods

The design of metal hydride storage systems requires a comprehensive understanding of the key thermodynamic and kinetic mechanisms. To effectively address the aforementioned thermal management challenges and to properly configure the thermal management system, it is essential to have a clear understanding of the variables involved in, and of the operating conditions. This chapter describes the methodological framework adopted to develop a mathematical model aimed at supporting the scale-up of a hydrogen storage system. The model has been designed to be applicable across different metal alloys and varying boundary conditions, providing temperature profiles as a function of hydrogen flow rate. The approach employed aims to balance the necessity for detailed, physically accurate descriptions with practical factors like model complexity and computational feasibility. By describing each stage of the modelling process, this section illustrates the governing equations and justifies the hypothesis assumed.

The model development draws on two main analyses: the chemical reaction of hydrogen absorption/desorption and the energy balances that describe heat transfer within the reactor. In particular, the equations governing the chemical process inside the reactor take into account the metal alloy thermophysical properties, such as activation/deactivation energies and formation enthalpy. The heat transfer analysis, on the other hand, is based on the fundamental principles of thermodynamics and the governing energy balances.

4.1 Assumptions

The model incorporates several assumptions to ensure both practicality and computational feasibility. Many of these assumptions are commonly adopted in the modelling of metal hydride storage systems [25], [30], [31], [32], [33]:

(i)   Hydrogen follows the ideal gas law: this assumption is justified by the moderate pressure and temperature conditions typically encountered in metal hydride storage systems, where deviations from ideal gas behaviour are minimal.

(ii)   The metal hydride alloy is homogeneous and isotropic: the metal alloy is assumed to have uniform composition throughout the reactor and uniform properties in all directions. This assumption facilitates the thermal and kinetic calculations, avoiding

the complexity of a detailed microstructural model. The metal hydride bed is also presumed to exhibit uniform porosity.

(iii) Gas pressure distributes promptly and homogenously within the system:

    a. Gas velocity effects are neglected

    b. The reactor is small in scale and packed with relatively large metal hydride grains

    c. Pressure variations are considered negligible, leading to the omission of heat transfer by mass convection.

(iv) Local thermal equilibrium: the temperature of the hydrogen gas is considered equal to that of the surrounding hydride bed, allowing for a single energy balance equation to describe heat transfer.

(v) Radiative heat transfer is neglected: the system operates near ambient temperatures

(vi) The dependence of equilibrium pressure on hydrogen concentration is neglected: the pressure-composition-temperature (PCT) relationship is simplified by assuming that equilibrium pressure is only a function of temperature.

(vii) Thermal and physical properties of the bed are considered constant: the effective thermal conductivity, specific heat capacity, and other material properties are assumed independent of both temperature and hydrogen concentration within the bed, and pressure variations.

(viii) Structural variations within each control volume are negligible: the reactor is divided into control volumes that are assumed to have uniform properties, eliminating the need to account for local structural variations.

Several of the assumptions adopted in this model are widely accepted in the modelling of metal hydride storage systems, such as the ideal gas approximation and the negligible contribution of radiative heat transfer. The validity of these simplifications has been examined in literature, and different modelling approaches were compared to assess their impact on system behaviour [25]. Key assumptions, such as treating hydrogen as an ideal gas, assuming local thermal equilibrium, and neglecting heat transfer by mass convection, have been tested under typical operating conditions. In particular, the assumption of hydrogen behaving as an ideal gas has been evaluated by comparing pressure predictions obtained using both ideal and non-ideal gas formulations over a relevant range of temperatures and pressures. The findings indicate that, while minor deviations occur at high pressures, the assumption remains valid within the operating conditions relevant to

metal hydride storage, as no significant differences were observed in hydriding rates or temperature evolution [25], [30].

Another common simplification in the modelling of metal hydride tanks is the assumption that gas movement within the bed has a negligible effect on heat transfer. This leads to the formulation of a conductive model, as opposed to a convective model, where heat transfer is primarily governed by conduction through the solid matrix rather than by hydrogen flow. Since the gas velocity in a porous medium is directly related to the pressure gradient, this assumption inherently implies that the effect of pressure variation is also neglected [34]. The validity of this approximation has been investigated in previous studies which compared temperature distributions obtained by solving the governing equations with and without the mass convection term. Their findings indicated that the difference in predicted temperatures was less than 1%, demonstrating that the omission of mass convection has a negligible effect on the overall thermal behaviour of the system. As a result, neglecting the role of gas movement in heat transfer, and consequently its effect on metal hydride performance, is considered a reasonable approximation for modelling purposes [25], [35].

These assumptions are introduced to simplify the computational framework while ensuring that the model effectively represents the fundamental physical and thermodynamic processes governing hydrogen absorption and desorption in metal hydrides. Although certain approximations may introduce limitations, they remain justified within the context of reactor design and optimization. More complex models could account for spatial temperature variations, material inhomogeneities, and time-dependent behaviours, but such complexity would be unnecessary for the design goals of this study, where the focus is on a first-order estimation of performance. By balancing accuracy with computational feasibility, these simplifications align with practical manufacturing considerations. Further refinements will be introduced in the subsequent modelling steps to enhance the model's predictive capabilities where necessary.

4.2 Energy storage capacity and density

The total energy that can be stored in the reactor is estimated by considering the effective volume that is available for the metal hydride alloy, as well as the hydrogen absorption capacity of the alloy that has been selected.

A cylindrical shape of the reactor has been modelled as a straightforward and reliable option for metal hydride storage [34]. The gross internal volume of the cylindrical vessel (V_{cyl_in}) is taken as the initial point, from which the volume occupied by any internal diffuser or structural supports is deducted (V_{diff}), resulting in the net reactor volume:

$$V_{net} = V_{cyl_{in}} - V_{diff} \quad (4)$$

Metal hydrides typically experience a volumetric increase during the transition of the alloy from its unhydrided to its hydrided state. To ensure there is enough free volume for the alloy to expand when fully hydride, the effective volume of alloy that can be used to load the reactor is further corrected by a volumetric expansion coefficient. Defining α as the fractional increase in the alloy's volume upon full hydriding, the volume effectively occupied by the hydride can be expressed as:

$$V_{eff} = \frac{V_{net}}{1+\alpha} \quad (5)$$

This relationship assumes that any expansion in the hydrided phase reduces the practical loading volume in a uniform manner. However, the degree to which expansion plays a role depends heavily on how the system is physically constrained and how the packing of the powdered alloy or pellets is arranged inside the vessel. In simplified design practice, rather than relying on the exact volumetric expansion ratio of the material, a commonly adopted engineering approach is to allocate a certain fraction - often in the range of 20 to 30 percent - of the reactor's gross volume as "free space". This conservative allowance effectively accommodates the expansion of the hydrided material and any packing rearrangements, without necessitating detailed microstructural or packing-level calculations. Although this strategy may not precisely capture every nuance of volumetric growth, it offers a practical and robust way to ensure that neither the mechanical integrity of the system nor its hydrogen storage performance are compromised under full loading conditions.

Once V_{eff} is known, it is multiplied by the alloy's bulk density ρ_{alloy} to find the mass of the alloy placed in the reactor:

$$m_{alloy} = \rho_{alloy} \cdot V_{eff} \quad (6)$$

The fraction of hydrogen that the alloy can absorb under equilibrium conditions is given in weight percent (wt.%). The mass of hydrogen stored is calculated through the definition of weigh percent capacity:

$$wt.\% = \frac{m_{H_2}}{m_{alloy} + m_{H_2}} \cdot 100 \qquad (7)$$

The resulting hydrogen mass is then multiplied by the lower heating value (LHV) of hydrogen to obtain the total chemical energy stored:

$$E_{stored} = m_{H_2} \cdot LHV_{H_2} \qquad (8)$$

The volumetric energy density is calculated dividing the energy stored by the reactor's gross internal volume (or by any other relevant reference volume):

$$\rho_{energy} = \frac{E_{stored}}{V_{cyl_{in}}} \qquad (9)$$

4.3 Kinetic modelling of hydrogen chemisorption

The mathematical framework governing the modelling of hydrogen storage systems is independent of the specific metal hydride material employed. However, the accurate representation of key phenomena, such as the kinetics of hydrogen interaction with the storage medium, necessitates the incorporation of material-specific properties. Consequently, while the fundamental equations remain unchanged across different metal hydride alloys, the parameter values must be carefully selected to reflect the characteristics of the system under study.

The process of chemisorption is well described by the van't Hoff equation (2) that relates the equilibrium plateau pressure to the temperature. The equation previously introduced is here reported to maintain clarity and coherence within this section:

$$ln\left(\frac{P_{eq}}{P_0}\right) = -\frac{\Delta H}{R\,T} + \frac{\Delta S}{R} \qquad (2)$$

The reaction kinetics are governed by an Arrhenius-type equations, (10) and (11) respectively for absorption and desorption. The intrinsic properties of the material are incorporated through the Arrhenius term (Equation 3). The equations express the rate as a function of temperature and pressure, which act as the driving forces:

$$\dot{m}_a = C_a \cdot exp\left(-\frac{E_a}{R\,T}\right) \cdot ln\left(\frac{P}{P_{eq}}\right) \cdot (\rho_{ss} - \rho_s) \quad (10)$$

$$\dot{m}_d = C_d \cdot exp\left(-\frac{E_d}{R\,T}\right) \cdot \left(\frac{P - P_{eq}}{P_{eq}}\right) \qquad (11)$$

Where C_a and C_d are pre-exponential factors, E_a and E_d is the absorption and desorption activation energies, ρ_{ss} is the density of the metal-hydride at the end of absorption (saturated density) and

ρ_s is the density of the solid without hydrogen. P is the hydrogen pressure and P_{eq} is the equilibrium pressure of the MH system.

The calculation of the total heat released (or absorbed) and the resulting thermal power when hydrogen reacts exothermically with a metal hydride can be performed through the equation:

$$Q_{reaction} = n_{H_2}\Delta H \qquad (12)$$

Where ΔH is the molar enthalpy of hydride formation (J/mol) and n_{H2} is the number of moles of hydrogen reacted.

In order to determine the thermal energy released by absorbing 1 kg of hydrogen, it is useful to note that hydrogen possesses a molar mass of approximately 2.016 g /mol. Consequently, 1 kg of hydrogen corresponds to roughly 496 moles of H_2. The total energy involved in the reaction can then be estimated by multiplying this mole quantity by the molar enthalpy of hydride formation (ΔH).

By considering the instantaneous molar flow rate of hydrogen reacting with the metal, then the rate at which heat is generated can be expressed as:

$$\dot{Q}_{gen} = \dot{n}_{H_2}\Delta H \qquad (13)$$

Where $\dot{Q}_{gen}$ is the thermal power (W) released and $\dot{n}_{H_2}$ is the molar absorption rate (mol/s).

Equation 12 emphasises the coupling between kinetics and thermal effects, which in turn underlines the need for effective thermal management. The subsequent sections will provide a comprehensive examination of the modelling of heat removal through conduction, convection, or dedicated cooling elements. The focus of these sections will be on the governing equations for heat transfer in hydrogenation reactors.

The rate of reaction is inherently limited by temperature, pressure, and the hydrogen content within the reactor. The difference between the equilibrium pressure and the system pressure is the driving force of the sorption processes. Lower equilibrium pressure for the same system pressure causes increased hydrogen absorption and faster formation rate and similarly a higher equilibrium pressure for the same system pressure enhances the desorption. Because of the direct relationship between temperature and equilibrium pressure, effective thermal management is required to prevent the reaction from inhibiting itself. Cooling the system during absorption and heating during desorption, helps to increase the reaction rates [25], [32], [33].

Furthermore, the dependence of the reaction rate on the hydrogen content within the material is taken into account. The term (ρ_{ss} - ρ_s) represents the difference between the final saturated density of the metal hydride and the density of the unhydrided solid. As hydrogen absorption approaches saturation, the number of available interstitial sites within the alloy decreases, leading to a gradual reduction in the reaction rate. A common strategy adopted by similar models is to define a dimensionless variable X indicating the fraction of hydrogen absorption completed. The representation of this phenomenon allows the model to more accurately reflect the actual physical process. This level of detail can become important to capture the nuances of partial saturation or cycle performance over long periods. However, alternative models often employ the more elementary Arrhenius-type velocity expression. This approach has frequently been found to be adequate for a 0D or lumped-parameter approach that prioritises the primary driving factor (pressure difference from equilibrium).

Since the objective of this study is to provide a design-oriented modelling tool, it is necessary to consider the worst-case scenario, which corresponds to the maximum heat generation within the system. This condition occurs when the reaction rate is at its peak, meaning that the driving force for absorption is at its maximum. Such a scenario takes place in the initial phase of hydrogen absorption, when the metal hydride bed is fully unhydrided, and the number of available interstitial sites for hydrogen incorporation is at its highest. Under these conditions, the exothermic reaction proceeds with maximum intensity, leading to the highest thermal load on the system. This modelling approach provides a conservative design basis, allowing the system to be dimensioned for the most demanding operational conditions. By ensuring that the cooling system can handle the peak load, it is possible to guarantee stable performance across any range of operating scenarios with lower demand.

4.4 Thermal modelling and heat transfer analysis

The heat transfer model developed in this study describes the steady-state thermal behaviour of the metal hydride reactor. The model accounts for heat generation within the hydride bed, radial heat conduction through the reactor shell, and convective heat dissipation to the surrounding cooling fluid. The system is modelled with a cylindrical geometry, where heat transfer is assumed to be exclusively radial, with no axial or circumferential variations.

The model assumes local thermal equilibrium (iv) within the hydride bed, meaning that the solid and gas phases are at the same temperature. Convective and radiative heat transfer mechanisms

within the hydride bed have been neglected, leading to a purely conductive heat transfer model in the region where chemical heat generation occurs.

4.4.1 Assumptions and control volume definition

I.   Steady-state conditions

II.   Radial one-dimensional conduction

III.   Homogeneous volumetric energy generation

IV.   Constant properties

To clearly illustrate the thermal regions considered in this model, the control volume is schematically represented in Figure 4-1 and it includes:

- The hydride bed ($r_0 \leq r \leq r_1$), where heat is generated due to the exothermic reaction of hydrogen absorption, and it is transferred through conduction
- The reactor shell ($r_1 \leq r \leq r_2$), which serves as a conductive medium with no internal heat generation

At the external surface of the shell heat is removed by convective heat transfer by means of a cooling fluid.
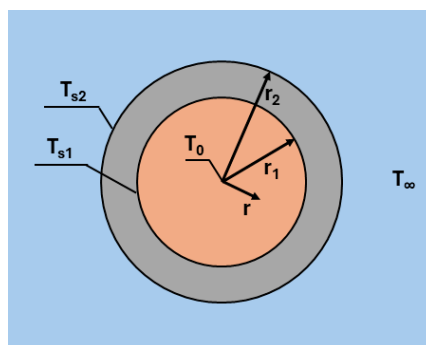
Figure 4-1 Schematic representation of the control volume.

4.4.2 Governing equations

As the system in evaluated under steady-state conditions, the energy balance equation can be written as:

$$\dot{Q}_{gen} = \dot{Q}_{conv} \qquad (14)$$

Where Q_{gen} is the thermal power generated by the reaction, as seen in equation (13), and Q_{conv} is the heat removed by convection.

To determine the temperature distribution inside the reactor, the heat conduction equation, for a cylinder with internal heat generation, in steady-state conditions, and in cylindrical coordinates has been considered:

$$\left(\frac{1}{r}\right)\frac{d}{dr}\left[\lambda_e \, r\frac{dT}{dr}\right] + \dot{q} = 0 \qquad (15)$$

Where λ_e is the bed thermal conductivity (W/m K), T is the temperature distribution (K), r is the radial coordinate (m), and $\dot{q}$ is the volumetric heat generation rate (W/m³).

The fourth assumption, which states that the thermal conductivity λ_e is considered constant, allows the governing equation to be expressed as:

$$\left(\frac{1}{r}\right)\frac{d}{dr}\left[r\frac{dT}{dr}\right] + \frac{\dot{q}}{\lambda_e} = 0 \qquad (16)$$

The third assumption, which states that the heat generation through the hydride is homogeneous, allows to express is as the thermal power generated by the reaction divided by the internal volume of the cylinder:

$$\dot{q} = \frac{\dot{Q}_{gen}}{V_{cyl}} \qquad (17)$$

Assuming uniform energy generation, the equation (16) can be integrated to obtain:

$$r\frac{dT}{dr} = -\frac{\dot{q}}{2\lambda_e} \, r^2 + C_1 \qquad (18)$$

The general solution to the distribution of temperature becomes:

$$T(r) = -\frac{\dot{q}}{2\lambda_e} \, r^2 + C_1 \ln r + C_2 \qquad (19)$$

To obtain C_1 and C_2 the following boundary conditions can be applied:

1. Symmetry: $\left.\frac{dT}{dr}\right|_{r=0} = 0$

    In cylindrical coordinates, the centreline of the reactor (i.e., at r=0) represents a geometric axis of symmetry. This means that the system is radially symmetric, and there is no preferred direction for heat flow along the axis.

2. Continuity: $T(r_1) = T_{S_1}$

   It set the temperature at the interface with the reactor shell.

Therefore, the temperature distribution is:

$$T(r) = T_{S_1} + \frac{\dot{q}r_1{}^2}{4\lambda_e}\left(1 - \frac{r^2}{r_1{}^2}\right) \qquad (20)$$

It can be noted from equation (20) that the temperature distribution as a parabolic behaviour within the hydride bed and the maximum value is at the centre (r=0):

$$T(0) = T_{S_1} + \frac{\dot{q}r_1{}^2}{4\lambda_e} \qquad (21)$$

The heat generated is then conducted through the reactor shell, which is modelled as a homogeneous solid with no internal heat generation. Thus, in steady-state conditions the temperature distribution follows the equation:

$$T(r) = \frac{T_{S_1} - T_{S_2}}{ln\left(\frac{r_1}{r_2}\right)} ln\left(\frac{r}{r_2}\right) + T_{S_2} \qquad (22)$$

By substituting this into Fourier's equation the expression for thermal resistance of a cylindrical wall is obtained:

$$R_{cond} = \frac{ln\left(\frac{r_2}{r_1}\right)}{2\pi \lambda_{steel}L} \qquad (23)$$

Where λ_{steel} is the steel thermal conductivity, and L is the cylinder length.

At the outer surface of the shell, heat is dissipated via forced convection to the cooling fluid, following Newton's law:

$$\dot{Q}_{conv} = h A_{ext} (T_{S_2} - T_\infty) \qquad (24)$$

Where h is the convective heat transfer coefficient (W/m² K), A_{ext} is the cylinder external surface (m²), and T_∞ is the temperature of the cooling fluid.

The thermal resistance due to convection is:

$$R_{conv} = \frac{1}{h A_{ext}} = \frac{1}{h 2\pi r_2 L} \qquad (25)$$

The heat transfer through the reactor shell and the heat transfer by convection can be modelled by the equivalent thermal circuit [Figure 4-2], and the thermal flux per unit of length can be expressed as:

$$q' = \frac{T_{S_1} - T_\infty}{R'_{cond} + R'_{conv}} \qquad (26)$$
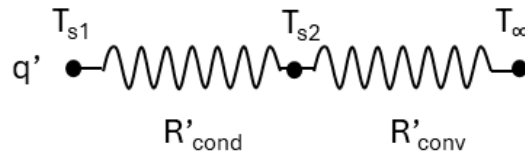
Figure 4-2 Equivalent thermal circuit.

The temperature at the interface between the hydride bed and the shell (T_{s1}) can be calculated as:

$$T_{S_1} = T_\infty + q'(R'_{cond} + R'_{conv}) \qquad (27)$$

Where:

$$q' = \dot{q}(\pi r_1{}^2) \qquad (28)$$

The effective thermal conductivity of a porous medium is influenced by several factors, including the thermal conductivities of the solid and fluid phases, the relative volume fractions of each phase, and the structural characteristics of the medium that determine the available pathways for heat diffusion. In the case of a metal hydride bed, which consists of a solid metal-hydride phase and a gaseous hydrogen phase, the medium is inherently discontinuous. The challenge in accurately determining the effective thermal conductivity arises from the complex interplay between these phases, particularly due to the significant difference in thermal conductivity between the solid and gas phases and the intricate pore structure that governs heat transport. Consequently, establishing a precise analytical expression for the effective thermal conductivity requires detailed knowledge of the phase distribution, pore structure, and interaction mechanisms. However, in the present study, rather than deriving an analytical model for the effective thermal conductivity - which would require precise knowledge of the volumetric

fractions and spatial distribution of each phase - a simplified approach has been adopted, consistent with established literature. The effective thermal conductivity of the bed is assigned a representative value, aligned with previous experimental and numerical studies on metal hydride systems with similar properties.

4.4.3 Convective heat transfer coefficient estimation

The convective heat transfer coefficient h quantifies the rate of heat exchange between the reactor shell and the surrounding cooling fluid. This coefficient is influenced by the fluid properties, flow conditions, and geometry of the system. In this section, the control volume of the model is extended to include not only the reactor but also the thermal bath in which the reactor is immersed, ensuring a comprehensive evaluation of heat dissipation [Figure 4-3].

In this model, the reactor is assumed to be cooled by an external transversal flow. The coefficient h is determined by empirical correlations based on dimensional numbers, in the case of a fluid moving perpendicular to the axis of a cylinder. The cylinder is assumed to have a diameter equivalent to the outside diameter of the reactor (D_2), with a uniform surface temperature (T_{s2}), cooled by a fluid at temperature T_∞, with an undisturbed current velocity (u_∞).

The Reynolds Number, which determines the flow regime, is given by:

$$Re = \frac{\rho \, u_\infty \, D}{\mu} = \frac{u_\infty \, D}{\nu} \quad (29)$$

Where ρ is the density of the fluid (kg/m^3), u_∞ is the velocity of the fluid (m/s), D is the characteristic diameter (m), μ is dynamic viscosity of the fluid (Pa·s) and ν is the kinematic viscosity of the fluid (m^2/s).

The Prandtl number can be calculated by:

$$Pr = \frac{c_p \mu}{\lambda_f} = \frac{\nu}{\alpha} \quad (30)$$

Where c_p is the specific heat capacity of the fluid (J/kg K), λ_f is the thermal conductivity of the fluid (W/m K), and α is the thermal diffusivity of the fluid (m^2/s).

Nusselt Number relates the convective heat transfer coefficient h to the thermal conductivity of the fluid through the equation:

$$Nu = \frac{h\,D}{\lambda_f} \qquad\qquad (31)$$

Two common correlations are available for computing the Nusselt Number. The Hilpert equation:

$$Nu = C\,Re^m\,Pr^{\frac{1}{3}} \qquad\qquad (32)$$

Where C and m are constants tabulated for different Reynolds Numbers.

The Churchill-Bernestein equation:

$$Nu = 0.3 + \frac{\left(0.62\,Re^{\frac{1}{2}}\,Pr^{\frac{1}{3}}\right)}{\left[\left(1+\left(\frac{0.4}{Pr}\right)^{\frac{2}{3}}\right)^{\frac{1}{4}}\right]} \cdot \left[1 + \left(\frac{Re}{282000}\right)^{\frac{5}{8}}\right]^{\frac{4}{5}} \qquad (33)$$

The Churchill-Bernestein equation is recommended in the case of [Re·Pr > 0.2].

The Hilpert correlation is simpler and widely used for forced convection over cylinders in cross-flow and it is appropriated when the velocity of the cooling fluid is known and the fluid regime can be reasonably estimated. In the case of uncertainty of fluid velocity, the Churchill-Bernstein correlation remains a more robust alternative, as it covers a wider range of flow conditions, including low-speed and mixed convection scenarios.

In this study, the reactor has been considered immersed in a controlled thermal bath, where the fluid motion can range from gently stirred to vigorously stirred conditions. The fluid velocity is unknown, it can vary across different ranges depending on the typology of thermal bath. Thermal baths are generally classified as:

- Gently stirred: fluid velocity in the range of 0.05 – 0.1 m/s, the flow is typically induced by weak circulation or low-speed agitation. The heat transfer mechanism can be considered also as a natural convection.
- Moderately stirred: fluid velocity around 0.1 – 0.2 m/s.
- Vigorously stirred: fluid velocity above 0.3 m/s. The flow is characterised by strong turbulence, promoting enhanced convective heat transfer.

Since the exact fluid velocity is not explicitly known, the system is initially assumed to operate within the gently to moderately stirred range, and the Churchill-Bernstein equation results to be more appropriate.
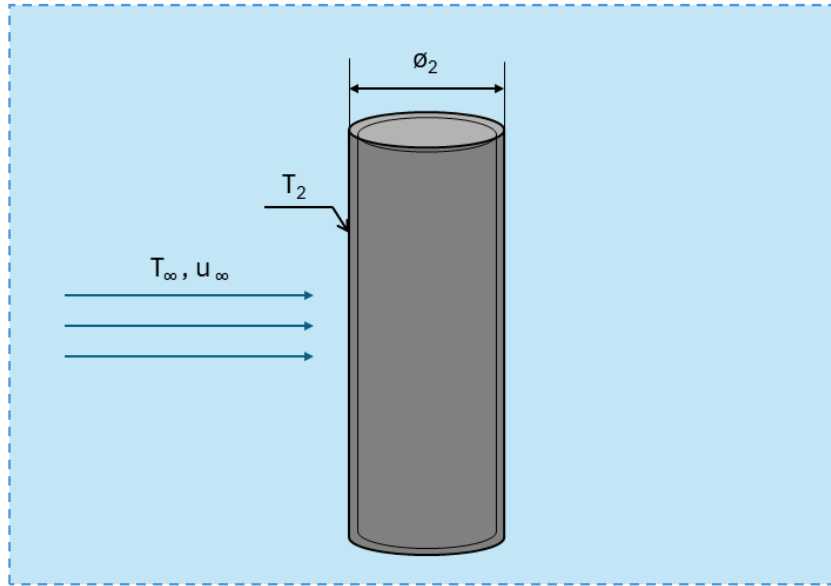
Figure 4-3 Geometry definition for the correlation of Nu, Pr and Re numbers.

In order to estimate the flow velocity, the cross-section of the thermal bath must be considered, given its geometric dimension [Figure 4-4]. The relationship between the fluid velocity and the volumetric flow rate is expressed as follows:

$$\dot{V} = S_{bath} \cdot u_\infty \qquad (34)$$

Where u_∞ is the fluid velocity (m/s), S_{bath} is the cross-section area of the thermal bath (m^2), and V is the volumetric flow rate (m^3/s).

The volumetric flow rate can be determined consider the density of the fluid (ρ) and the fluid mass flow rate (ṁ):

$$\dot{V} = \frac{\dot{m}}{\rho} \qquad (35)$$

In determining the fluid mass flow rate, the energy balance for the cooling fluid must be considered. At steady-state conditions, to ensure effective heat dissipation, the thermal power transferred from the reactor shell to the cooling fluid must be removed by the mass flow rate of the thermal bath. The energy balance is expressed as:

$$\dot{Q}_{conv} = \dot{Q}_{fluid} = \dot{m} c_p \Delta T \qquad (36)$$

Where ΔT is the temperature difference of the cooling fluid between the inlet and the outlet of the bath.

The temperature difference of the cooling fluid between its inlet and outlet is a crucial parameter, as it directly influences the effectiveness of the cooling system. In thermal bath applications, the temperature difference (ΔT) is typically maintained within a controlled range to ensure stable and efficient heat dissipation. The precise value of ΔT is contingent on the particular cooling requirements and the configuration of the system; however, it is generally maintained at low values to ensure uniform temperature control and to prevent excessive thermal gradients within the bath. In precision-controlled systems, such as laboratory thermal baths, a ΔT of 1 to 2 K is often employed to minimise fluctuations and ensure a highly stable thermal environment. This approach ensures homogeneous cooling and precise temperature regulation, which is essential in applications requiring stringent thermal control. The selection of an appropriate ΔT is of paramount importance, as the relationship between the mass flow rate of the cooling fluid and its temperature rise is governed by the energy balance equation (36). A smaller ΔT necessitates a higher coolant flow rate to ensure effective heat removal, whereas a larger ΔT allows for a lower flow rate while maintaining sufficient cooling capacity.

In the context of this study, the most appropriate value of ΔT is contingent on the operational constraints of the cooling system. While the theoretical framework presents the governing equations in a general form, the actual value of ΔT will be defined in the case study section, ensuring that it aligns with practical system requirements and the specific thermal management needs of the reactor.
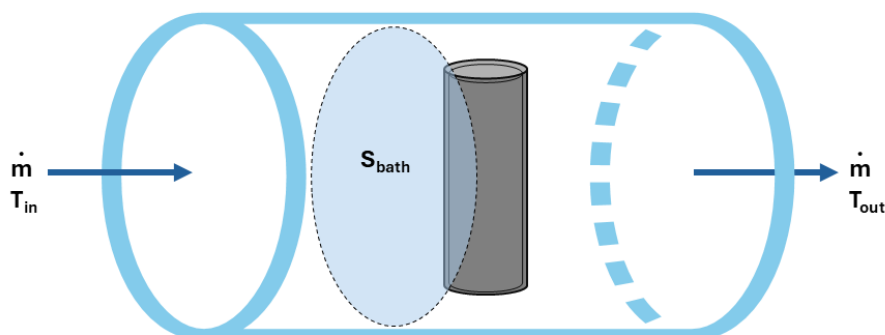
Figure 4-4 Cooling fluid and bath's section.

The final thermal model combines the equations related to the kinetics of the absorption/desorption reaction with those that describe heat flow through the material. These governing equations are not independent but interact such that the heat generated by the reaction influences the temperature, and the temperature in turn modulates the reaction rate. The overall energy balance within the reactor accounts for both the heat produced by the reaction and the heat transport by conduction in the material.

This approach combines the two analyses in steady-state conditions, assuming a 1D model. While real-world systems may involve more complex dynamics, this model provides a first-order approximation making it a practical tool for reactor design. The primary goal is to define key parameters such as energy storage capacity, energy density and temperature distribution, ensuring that the system remains in operation.

5   Case study

The developed model is designed to be applicable to various metal hydride alloys and adaptable to different boundary conditions. In particular, the mathematical framework has been implemented for a specific reactor geometry and thermal management configuration, ensuring a comprehensive evaluation.

In defining the geometry of the reactor and corresponding design targets, a cylindrical vessel is selected as a straightforward and reliable option for metal hydride storage in a stationary application [12], [25]. The target energy storage capacity for the reactor is set to approximately 1 kWh. The motivation behind the compact dimensions of the model is the intention to integrate multiple modules in order to achieve an enhanced overall capacity. However, the present study focuses on modelling the behaviour of a single reactor.

It is possible to adopt the one-dimensional radial heat transfer model, assuming negligible temperature gradients in both the axial and circumferential directions. The heat generated during hydrogen absorption can be treated as uniformly distributed across the cylinder's volume. This assumption is further strengthened if an internal hydrogen diffuser is employed, as it would foster more homogeneous gas distribution along the axial direction.

A temperature-controlled circulating bath is used to circulate the heat exchange fluid in order to add and remove heat to and from the tank during desorption and absorption. The choice of a thermal bath cooling system in this study is supported by findings from previous research, which indicate that for cylindrical metal hydride beds of dimensions comparable to those considered here, external cooling proves more effective than internal cooling in enhancing the dynamic performance of hydrogen uptake. This is attributed to the larger heat exchange area between the heat transfer fluid and the metal hydride. Additionally, this approach reduce manufacturing complexity and costs by eliminating the need for additional leak-proof penetrations required for internal heat exchangers [30].

The reactor is integrated ins Power-to-power system between an electrolyser and a fuel cell, which define its operating pressures. In this configuration, the electrolyser produces hydrogen, which is stored in the reactor under controlled conditions, and subsequently supplied to the fuel cell when needed for power generation.

The following sections present the specifications of the system components. The geometric parameters of the cylindrical reactor, the properties of the selected metal hydride alloy (TiFe), and the thermophysical properties of hydrogen and the cooling fluid are reported. These data are then used as input parameters for the numerical model.

The reactor consists of a cylindrical tube, sealed at both ends by flanges [Figure 5-1]. The material used is AISI316 stainless steel. The specifics are given in Table 5-1:
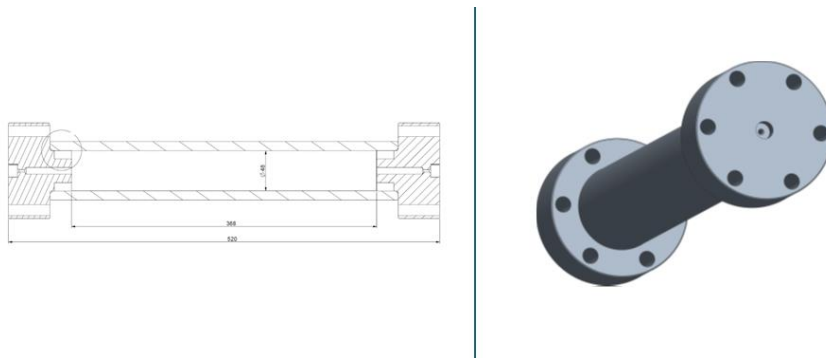
Figure 5-1 Reactor geometry.

Table 5-1 Reactor specifics.

Dimension	Symbol	Value	Unit of Measurement
Internal diameter	$\varnothing_i$	48	mm
External diameter	$\varnothing_e$	70	mm
Length	L_{cyl}	368	mm
Thermal conductivity	λ_{steel}	13.4	W / m K

The selected metal alloy is TiFe, its key parameters assumed are provided in Table 5-2 [27]:

Table 5-2 TiFe properties.

Property	Symbol	Value	Unit of Measurement
Reversible gravimetric capacity (at 25 °C)	w	1.31	wt.%
Density	ρ_s	6500	kg / m³

34

Saturation Density	ρ_{ss}	6600	kg / m^3
Coefficient of volumetric expansion	α	30	%
Thermal conductivity	λ_e	2.5	W/m K
ABSORPTION			
Enthalpy of formation	ΔH	24300	J / mol
Reaction entropy	ΔS	100	J / mol K
Energy of activation	E_a	21500	J / mol
Pre-exponential kinetic factor	C_a	25	1 / s
DESORPTION			
Enthalpy of formation	ΔH	27400	J / mol
Reaction entropy	ΔS	103	J / mol K
Energy of activation	E_d	19000	J / mol
Pre-exponential kinetic factor	C_d	15	1 / s

Relevant properties of hydrogen are provided in Table 5-3:

Table 5-3 H$_2$ properties.

Property	Symbol	Value	Unit of Measurement
Molar Mass	M	2.01	g/mol
Density (at STP)	ρ_{H2}	0.0899	kg /m^3
Lower Heating Value	LHV_{H2}	142	MJ/kg

In addition the following system reference have been assumed: Gas Constant R = 8.314 J / mol K and Reference Pressure P_0 = 1.013 bar.

The reactor installation between an electrolyser and a fuel cell defines hydrogen inlet and outlet pressure as:

- Inlet pressure (P_{in}) = 30 bar

- Outlet pressure (P_{out}) = 3 bar

The thermal management system is asked to guarantee a constant maximum operating temperature inside the reactor equal to 25 °C. The thermal management is performed by means of a precision thermal control bath. The operating fluid is water. Data of the thermal bath are provided in Table 5-4:

Table 5-4 Thermal bath operating point and water properties.

Property	Symbol	Value	Unit of Measurement
Bath controlled temperature	T_∞	7	°C
Bath section area	S_{bath}	0.06	m^2
ΔT operating fluid	ΔT	1 - 5	°C
Flow rate	V'	16 - 31	l/min

Since the cooling fluid temperature in the bath is set to 7°C (280.15 K), all relevant fluid properties have been evaluated at this temperature. The corresponding thermophysical data are presented in Table 5-5 [36].

Table 5-5 Water thermophysical properties from NIST [36].

Properties for Water at T = 280 K, P = 1 bar			
Density	ρ_{H2O}	999.91	kg / m^3
Specific heat	$c_{p,H2O}$	4.2009	kJ /kg K
Thermal conductivity	λ_{H2O}	0.57198	W/m K
Viscosity	μ_{H2O}	0.0014336	Pa·s

6 Results and discussion

This chapter presents the results obtained from the implementation of the case study data into the described model. The following results were generated using a computational model developed in Python. A custom solver was implemented to leverage Python's versatility in numerical simulations, data visualization, and computational efficiency, particularly when integrated with scientific libraries such as NumPy, SciPy, and Matplotlib. The analysis has been exclusively focused on the hydrogen absorption process, as it represents the most critical phase in terms of reaction kinetics and thermal management.

6.1 Energy storage capacity and density: results

The computational model begins by establishing the geometric parameters of the system and the weight percentage (wt.%) of the selected metal hydride alloy. These fundamental inputs enable the calculation of key performance indicators, including the total energy storage capacity and volumetric energy density of the system. This preliminary assessment provides essential insights into the storage potential of the hydrogen absorption process, allowing for an initial characterization of the system's efficiency. The results include the tank volume, the volume and mass of the TiFe alloy, the stored hydrogen mass, the overall system mass, and the corresponding energy storage values. They are presented in Table 6-1 as a basis for the subsequent analysis steps.

Table 6-1 Energy storage capacity and density results.

Results	Value	Unit of Measurement
Tank Volume	0.666	l
TiFe Volume	0.512	l
TiFe Mass	3.3295	kg
H_2 Capacity (mass)	0.0442	kg
Energy Stored	5.304	MJ
	1.473	kWh
Volumetric Energy Density	7964.3	MJ / m^3
	2212.3	kWh / m^3

6.2 Kinetic of hydrogen absorption: results

Given the thermophysical properties of the selected TiFe alloy, the reaction equilibrium can be characterized using the van't Hoff equation. By varying the operating temperature, the corresponding equilibrium pressures have been determined. The obtained data for TiFe are presented in Table X, while the van't Hoff plot, illustrating the relationship between $\ln(P_{eq})$ and $1/T$, is shown in Figure 6-1. By applying the kinetic model, the hydrogen absorption rate has been determined. Given the total hydrogen mass stored in the reactor calculate previously [Table 6-1], it is also possible to compute the absorption time required to reach equilibrium. Furthermore, by considering the enthalpy of formation of the metal hydride, the thermal power generated during the reaction has been evaluated. Additionally, the stored energy in the form of hydrogen chemical energy has been calculated based on its lower heating value (LHV). The results are summarized in Table 6-2.
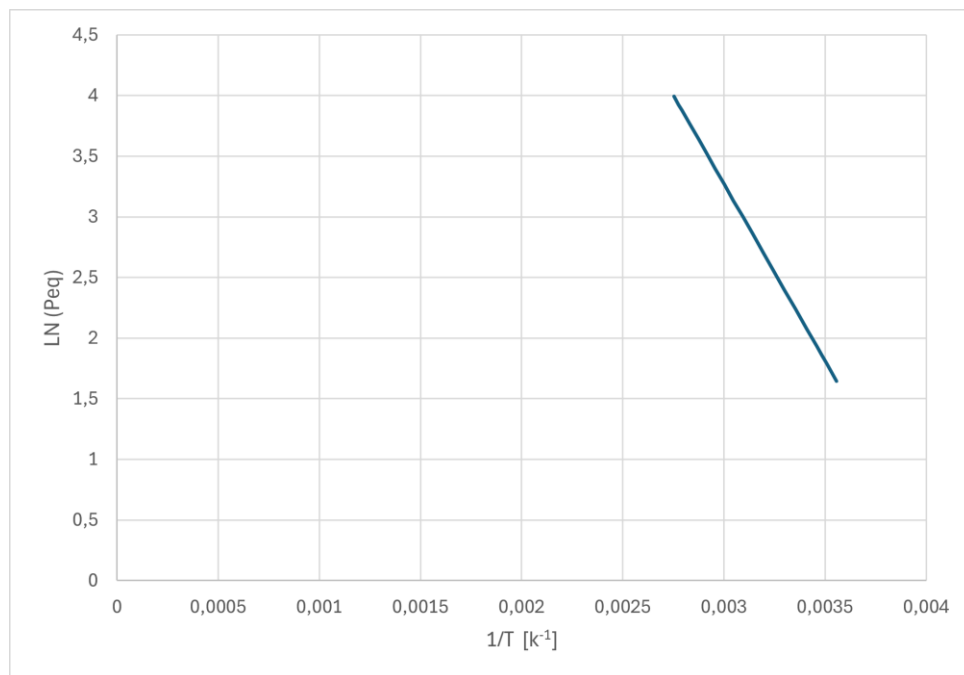
Figure 6-1 Van't Hoff diagram for TiFe.

Table 6-2 Kinetic of hydrogen absorption: results.

Temperature		Equilibrium Pressure	Rate$_{abs}$ per unit volume	Rate$_{abs}$	Time$_{abs}$	Thermal power generation	H$_2$ Power store
T [°C]	T[K]	P$_{eq}$ [bar]	m'$_{H2}$[kg/m³s]	m'$_{H2}$[kg/s]	t [s]	Q'$_{gen}$[kW]	P$_{store}$[W]
8	281,15	5,18	0,44	0,00023	194,10	2,74	27,32
10	283,15	5,58	0,45	0,00023	189,82	2,81	27,94
12	285,15	5,99	0,46	0,00024	186,05	2,86	28,51
14	287,15	6,44	0,47	0,00024	182,76	2,91	29,02
16	289,15	6,91	0,48	0,00025	179,96	2,96	29,47
18	291,15	7,40	0,49	0,00025	177,63	3,00	29,86
20	293,15	7,93	0,49	0,00025	175,80	3,03	30,17
25	298,15	9,37	0,50	0,00025	173,41	3,07	30,58
30	303,15	11,02	0,49	0,00025	174,56	3,05	30,38
35	308,15	12,88	0,48	0,00025	180,12	2,96	29,44
40	313,15	14,99	0,45	0,00023	191,92	2,78	27,63
45	318,15	17,36	0,40	0,00021	213,74	2,49	24,81
50	323,15	20,01	0,34	0,00017	254,63	2,09	20,83
55	328,15	22,97	0,25	0,00013	341,65	1,56	15,52
60	333,15	26,25	0,14	0,00007	607,37	0,88	8,73
65	338,15	29,89	0,00	0,00000	18925,00	0,03	0,28
70	343,15	33,90	-0,16	-0,00008	-529,72	-1,01	-10,01
75	348,15	38,31	-0,36	-0,00019	-237,49	-2,24	-22,33

These results indicate that the maximum acceptable temperature for the system is 65 °C, as it corresponds to a pressure of 29.89 bar. This value represents the critical threshold beyond which the reaction becomes self-inhibiting. The reason for this limitation is that the available hydrogen source from the electrolyser operates at 30 bar. Thus, exceeding this temperature would eliminate the pressure gradient, which serves as the driving force for the absorption kinetics. Without this pressure differential, the reaction can no longer proceed efficiently.

The values dictated by the kinetic at 25 °C are of particular interest, as this temperature represents the target operating point of the design. For the purpose of clarity, they are shown in Table 6-3.

Table 6-3 Results determined by reaction kinetic at 25 °C.

Temperature		Equilibrium Pressure	Hydrogen flow rate		Absorption Time	Thermal power generated	Power Store
°C	K	bar	kg/s	mol/s	s	kW	kW
25	298	9.37	0.000255	0.126404	173.4	3.07	30.58

6.3 Heat transfer model results

The thermal power generated by the absorption reaction, as determined in the previous section, serves as the input parameter for the heat transfer model. This thermal energy is then used to compute the volumetric heat generation rate inside the reactor.

The acceptable range for temperature difference (ΔT) and mass flow rate of the thermal bath was considered. Initially, a ΔT of 2 K was defined as a reference value. Based on this assumption, the required mass flow rate of the cooling fluid necessary to remove the generated heat was determined to be 0.3656 kg/s, equivalent to 21.94 l/min. This value falls within the operational range of the cooling system, confirming that the proposed thermal management solution is suitable for ensuring effective heat dissipation.

The computed mass flow rate of the cooling fluid determines a fluid velocity within the thermal bath of 0.0061 m/s. Given the system geometry, the corresponding convective heat transfer coefficient has been calculated to be 190.97 W/m^{2}K.

By plotting the temperature T as a function of the radial coordinate r, based on the volumetric heat generation rate obtained from the reaction kinetics, it is possible to visualize the thermal profile within the system [Figure 6-2]. It is observed that the temperature inside the reactor, for the given thermal power generation, is significantly higher than the design-specified operating conditions. In particular, the maximum temperature at the centre of the reactor (r=0) reaches 781.99 K (508.84 °C), while at the interface with the reactor shell (r=24 mm), the temperature is 518.08 K (244.93 °C). On the external surface of the reactor (r=35 mm), the temperature decreases to 478.90 K (205.83 °C).

These operating conditions are not acceptable for the system, as the temperatures reached within the reactor exceed the threshold at which the absorption reaction can proceed. At these elevated

temperatures, the equilibrium pressure of the hydride approaches or exceeds the pressure of the hydrogen supply from the electrolyser, leading to a self-inhibition of the reaction.
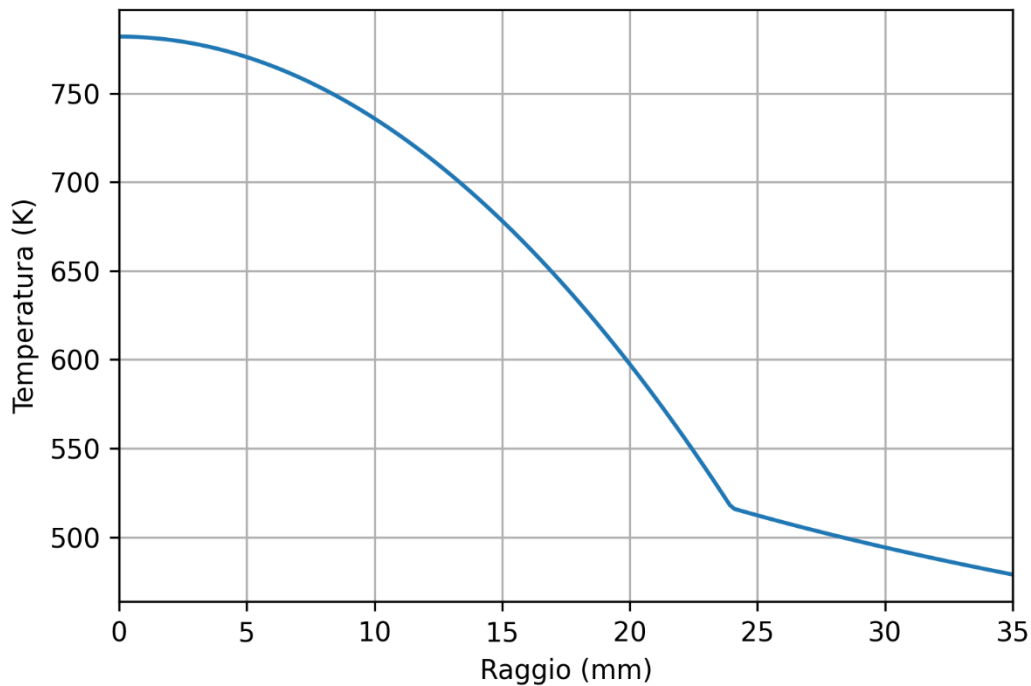
Figure 6-2 Temperature distribution within the reactor as a function of the radial coordinate, corresponding to the absorption rate determined by reaction kinetics.

In order to guarantee that the system functions within the requisite thermal limits and achieves the desired absorption efficiency, it is necessary to adjust the operating conditions. This may entail enhancing the cooling capacity of the thermal bath, reducing the hydrogen inlet flow rate, or modifying the reactor's heat dissipation design.

The thermal bath has an operational range of ΔT from 1 to 5 K and can handle a coolant flow rate between 16 and 31 l/min. Considering water as the cooling fluid with a specific heat capacity of 4.2009 kJ/kg·K, the maximum heat removal capacity is 10.85 kW. Therefore, its cooling capacity is not a limiting factor for the system. However, while the cooling system is adequately dimensioned, its operating conditions can be adjusted to enhance convective heat transfer between the coolant and the reactor. The fluid flow rate is a key controllable parameter, as it directly influences the fluid velocity inside the bath and, consequently, the convective heat transfer coefficient. To identify the optimal operating condition, an analysis has been conducted on the variation of the convective heat transfer coefficient as a function of the cooling fluid flow

rate. For the developed model, the convective heat transfer coefficient (h) is found to increase with the Reynolds number (Re), which, in turn, increases as the fluid velocity rises. Since fluid velocity is directly dependent on the flow rate, it follows that a higher flow rate leads to enhanced convective heat transfer. Consequently, it is reasonable to assume that at the maximum flow rate allowed by the cooling system, the convective heat transfer coefficient reaches its highest value, resulting in the most favourable heat dissipation condition for the given reactor geometry. This suggests that operating the cooling system at its upper flow rate limit would optimize thermal management.

In order to investigate this condition, the analysis was conducted by fixing the flow rate at its maximum value of 31 l/min. For the same thermal power considered previously, this corresponds to a temperature difference (ΔT) of approximately 1.42 K. Given these modified operating conditions, the convective heat transfer coefficient has been calculated to be 226.77 W/m^{2}K.

By plotting the temperature distribution as a function of the radial coordinate, it has been obtained the profile is shown in Figure 6-3. A slight improvement is observed compared to the previously analysed scenario; however, the conditions still do not reach the design target. In particular, the temperature at the centre of the reactor (r=0) is 750.62 K (477.47 °C), while at the interface with the reactor shell (r=24 mm), the temperature is 486.71K (204.32 °C). On the external surface of the reactor (r=35 mm), the temperature is 447.53 K (174.38 °C). In addition to not meeting the stipulated design requirements, these temperatures exceed the threshold at which the reaction becomes self-inhibiting. It is therefore necessary to adjust additional operating parameters to maintain a feasible absorption process.
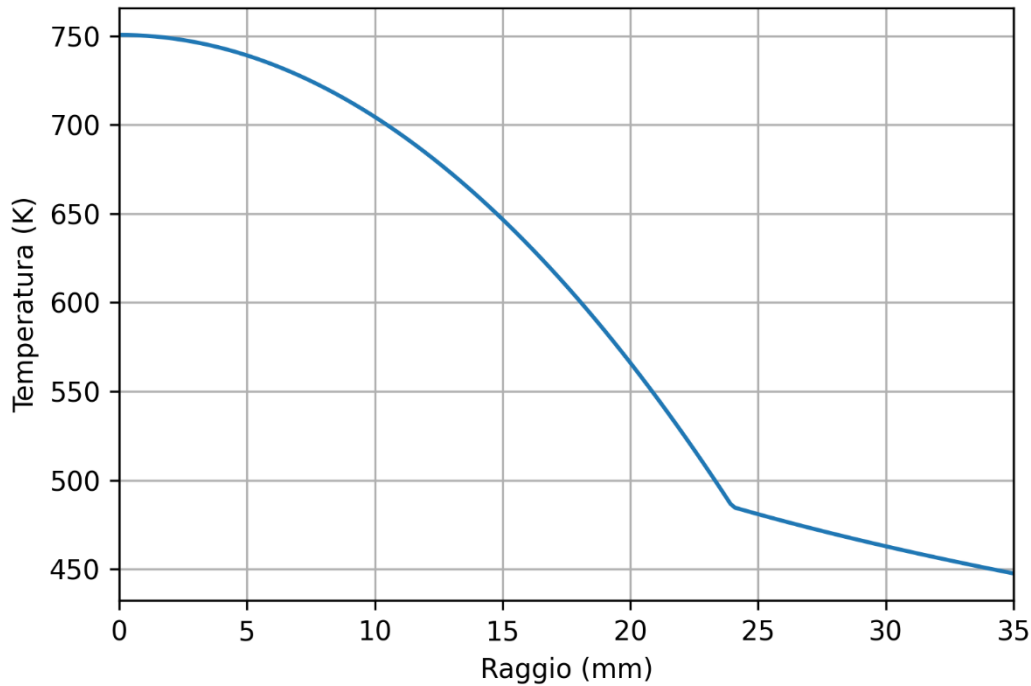
Figure 6-3 Temperature distribution within the reactor as a function of the radial coordinate r for the maximum coolant flow rate, corresponding to the highest convective heat transfer coefficient.

Since the reactor design cannot be modified to improve thermal dissipation, the focus shifts to regulating the hydrogen absorption rate. It has been observed that as the rate of hydrogen absorption decreases, the thermal power generated also decreases, leading to a reduction in internal reactor temperature. Figure 6-4 illustrates the temperature distribution within the reactor as a function of the radial coordinate r, analysed over a hydrogen flow rate range from 0 to 0.1264 mol/s (the kinetically determined maximum rate), with the flow rate values considered on a logarithmic scale.

In particular, it has been determined that the maximum allowable hydrogen flow rate to ensure a maximum reactor temperature of 298.76 K (25.61 °C) at r=0 is 1.28 e-03 mol/s [Figure 6-5]. The corresponding temperature distribution as a function of the radial coordinate under these optimized conditions is shown in Figure 6-6, illustrating the improved thermal behaviour achieved by adjusting the hydrogen absorption rate. This result confirms the theoretical assumption that the absorption reaction is not fundamentally limited by the intrinsic properties of the metal alloy, but rather by the efficiency of heat dissipation.
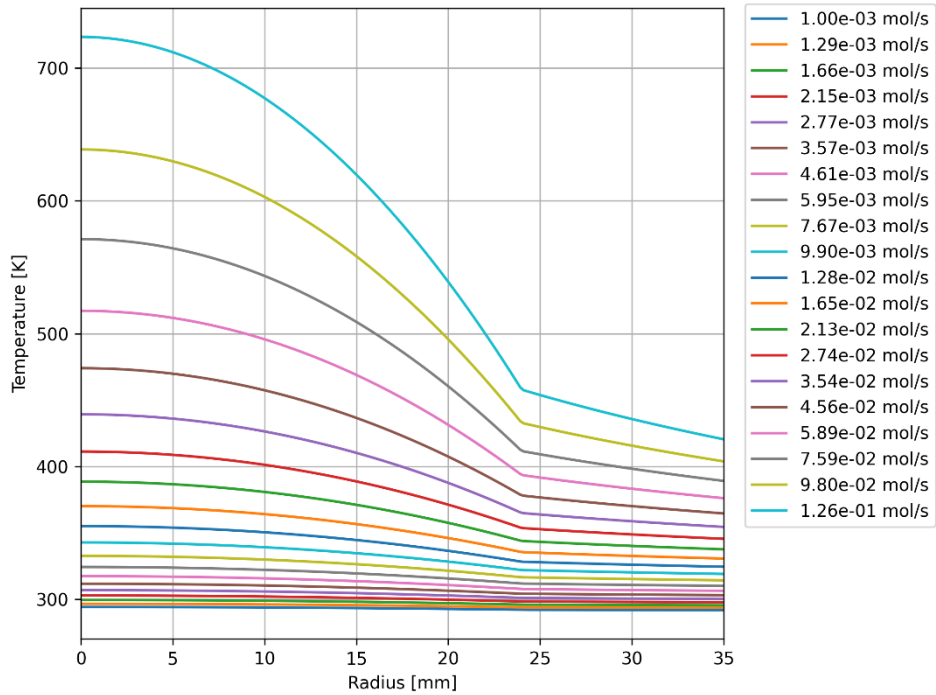
Figure 6-4 Temperature distribution within the reactor as a function of the radial coordinate r, analysed over a hydrogen flow rate range from 0 to 0.1264 mol/s (the kinetically determined maximum rate), with the flow rate values considered on a logarithmic scale.
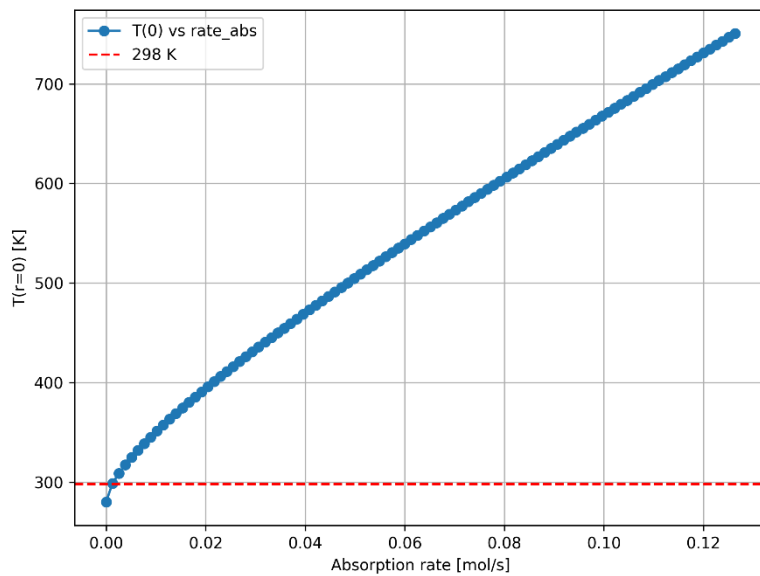
Figure 6-5 Temperature at the centre of the reactor (r=o) as function of the hydrogen absorption rate.
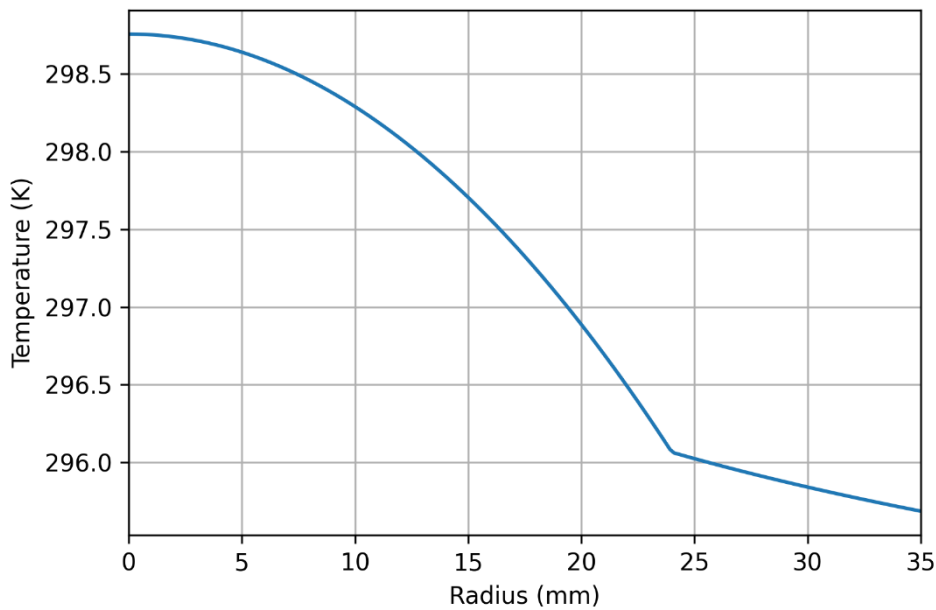
Figure 6-6 Temperature distribution within the reactor as a function of the radial coordinate r for the reduced hydrogen flow rate, ensuring a maximum reactor temperature around 298 K at r=0.

For this last case, where the hydrogen flow rate is reduced to $1.28 \cdot 10^{-3}$ mol/s, the corresponding thermal power generated is 31.10 W, and the absorption time is about 285 min. The volumetric flow rate of the coolant required to maintain these conditions is 0.313 L/min. Under these conditions, the temperature at the interface with the reactor shell (r=24 mm) is 296.08 K (22.93 °C), while at the external reactor surface (r=35 mm) it is 295.69 K (22.54 °C).

It can be hypothesised that slightly higher hydrogen flow rates could be permissible, given the assumption that the temperature inside the reactor is homogeneous, representing an average of the values plotted along r. However, the most conservative condition has been considered by evaluating the temperature at r=0.

Since the calculated hydrogen flow rate required to maintain the reactor temperature at 298 K is relatively small, and given that the absorption reaction can still proceed at higher temperatures, it is useful to explore the system's behaviour under less restrictive thermal constraints. To further investigate this, the analysis has been extended by setting the temperature limit at T(r=0) = 333 K (60 °C) [Figure 6-7]. This allows for a better understanding of how the system responds to an increased thermal threshold and how it affects the hydrogen absorption rate and thermal power generation.
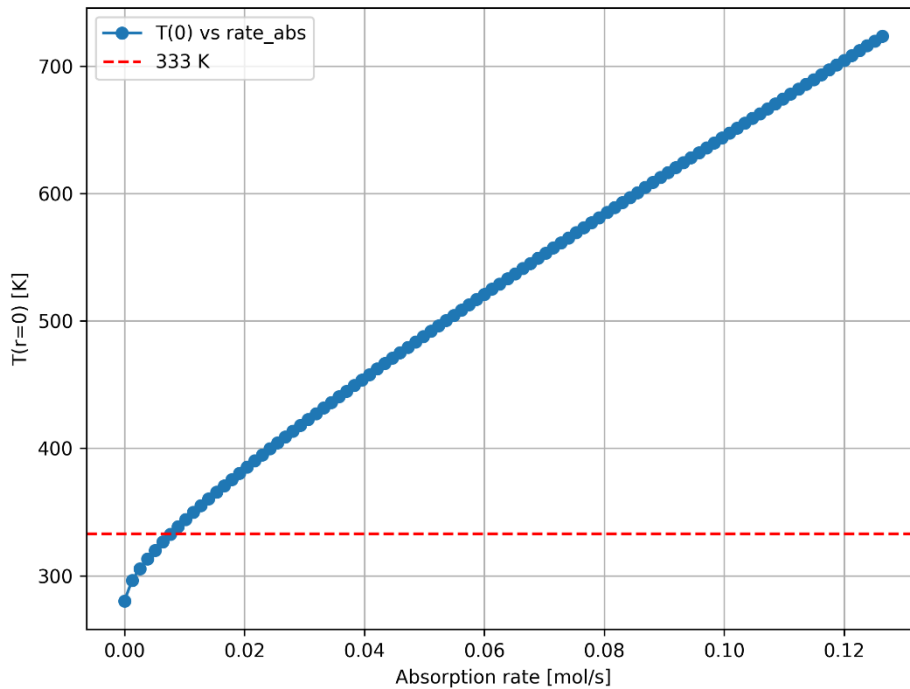
Figure 6-7 Temperature at the centre as function of hydrogen absorption rate, identifying the absorption rate corresponding to T(r=0)=333 K.

The hydrogen absorption rate at which the central reactor temperature (T_0) approaches 333 K is $7.66 \cdot 10^{-3}$ mol/s, corresponding to a thermal power generation of 186.14 W. Under these conditions, the temperature distribution within the reactor has been evaluated to assess the thermal behaviour of the system. The resulting temperature profile in Figure 6-8 shows that at r=0 the temperature is 332.56 K, while at the interface with the reactor shell (r=24 mm), the temperature decreases to 316.57 K. On the external surface of the reactor (r=35 mm), the temperature is 314.20 K. To sustain this operating condition, the required volumetric flow rate of the coolant is determined to be 2.66 l/min. This distribution highlights the thermal gradient across the system when operating at a higher allowable temperature threshold. At 333 K, the system operates within the temperature constraints required for the absorption reaction, ensuring that the process remains thermodynamically feasible. However, the calculated absorption rate of $7.66 \cdot 10^{-3}$ mol/s is significantly lower than the maximum rate allowable by reaction kinetics, which is $3.70 \cdot 10^{-2}$ mol/s. This indicates that the actual absorption rate is dictated by thermodynamic limitations rather than kinetic constraints, reinforcing the hypothesis that thermal dissipation is the primary limiting factor of the system. The inability to effectively remove heat prevents the

reaction from proceeding at its full kinetic potential, further confirming that enhancing heat transfer remains the key challenge for improving system performance. With this absorption rate, the absorption time is significantly reduced to 47.7 minutes, making this condition feasible for applications where a shorter absorption time is desired, while still ensuring that the system operates within acceptable thermal constraints.
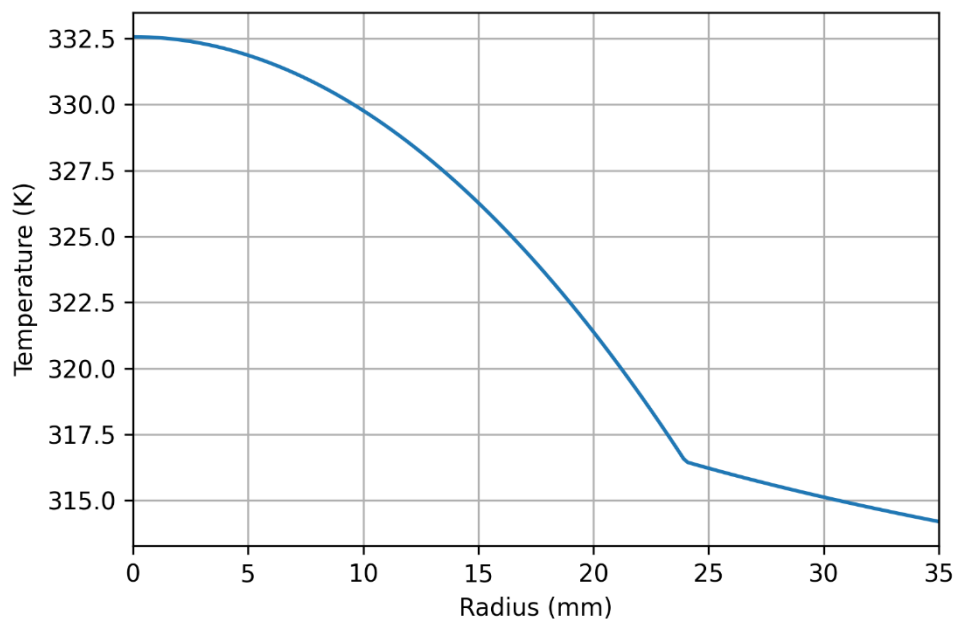
Figure 6-8 Temperature distribution within the reactor as a function of the radial coordinate r for the increased temperature limit of T(r=0)=333 K

The results obtained are consistent with other studies found in the literature that focus on the use of $LaNi_5$ as a hydrogen storage alloy. Notably, this alloy has been widely studied due to its favourable hydrogenation properties, and its reaction enthalpy ΔH is comparable to that observed in this study [12]. To further validate the model, it would be highly beneficial to compare it with experimental data obtained through dedicated testing. Performing controlled experiments would allow for a direct assessment of the model's predictive accuracy, providing insights into potential discrepancies and enabling refinements that enhance its reliability.

Some inherent limitations of the model must be acknowledged. The developed framework assumes steady-state conditions, meaning that transient effects, such as heat accumulation and time-dependent variations in temperature and pressure, are not explicitly accounted for. Additionally, due to the influence of reaction kinetics, heat generation exhibits significant spatial

variations within the reactor. While the current model provides valuable insights, a 2D or 3D approach would better capture temperature gradients and localized thermal effects. Furthermore, thermal conductivity has been assumed constant, whereas in real metal hydride beds, it varies with hydrogen loading, bed compaction, and structural degradation over time. Incorporating a sensitivity analysis on this parameter could enhance the model's accuracy and predictive reliability, allowing for a more comprehensive assessment of heat transfer dynamics under varying operational conditions. Future research should focus on enhancing heat transfer within the reactor by exploring alternative reactor designs, advanced cooling strategies, and the integration of high-conductivity materials into the hydride bed.

This study has provided a comprehensive analysis of the thermodynamic and kinetic behaviour of hydrogen absorption in metal hydrides. The findings confirm that thermal dissipation, rather than intrinsic reaction kinetics, is the primary limiting factor for system operation, emphasizing the critical role of effective heat management in optimizing performance. Beyond identifying operational constraints, this study highlights opportunities for improvement, demonstrating that by optimizing heat transfer strategies and regulating hydrogen absorption rates, it is possible to achieve stable and efficient system performance. Overcoming the challenges of thermal management through innovative reactor designs, improved cooling strategies and integration of highly conductive materials will be key to unlocking the full potential of metal hydrides for hydrogen storage. By building on these findings, metal hydrides can become a viable and competitive solution in the ongoing energy transition and play a critical role in the development of efficient, scalable and sustainable hydrogen storage technologies.

7 Conclusions

This thesis presents the development of a mathematical model aimed at supporting the scale-up of a hybrid hydrogen storage system. The design of metal hydride storage requires a comprehensive analysis based on its thermophysical properties, including activation/deactivation energy, enthalpy of formation, equilibrium pressure, reaction kinetics, and the external thermal management system. The developed model has been designed to be applicable to different metal alloys and boundary conditions. It provides temperature profiles as a function of the hydrogen flow rate, analysing the heat fluxes through the reactor.

In particular, the study has focused on the case of a cylindrical reactor placed between an electrolyser and a fuel cell for stationary applications. For the proposed reactor geometry, it has been observed that the hydrogen inlet flow rate must be reduced compared to the maximum allowable rate dictated by reaction kinetics alone, in order to ensure proper thermal regulation. The absorption rate of the kinetics is $1.264 \cdot 10^{-1}$ mol/s, corresponding to a thermal power generation of 3.07 kW. However, the analysis has shown that this thermal power cannot be fully dissipated by the reactor in the investigated case study, highlighting the need for more effective thermal management strategies. A key finding of this study is the importance of controlling the inlet flow rate during the absorption process. It was observed that reducing the flow rate limits heat generation, allowing the system to maintain a stable operating temperature of approximately 25°C. This result is crucial to ensure process stability and prevent the absorption reaction from self-limiting due to excessively high temperatures.

The developed model is well suited for steady-state thermal analysis of a metal hydride reactor operating under worst-case heat generation conditions. The alignment with existing research reinforces the validity of the modelling approach and highlights the relevance of the findings. To further validate the model, it would be highly beneficial to compare it with experimental data obtained through dedicated testing. Performing controlled experiments would allow for a direct assessment of the model's predictive accuracy, providing insights into potential discrepancies and enabling refinements that enhance its reliability.

The model developed assumes steady-state conditions, meaning that transient effects such as heat accumulation and time-dependent variations in temperature and pressure are not explicitly considered. Given the inherently dynamic nature of hydrogen absorption and desorption, a

transient model could provide a more comprehensive understanding of the system's behaviour, particularly in capturing the impact of heat transfer delays and kinetic constraints over time. Furthermore, the current model does not explicitly consider spatial inhomogeneities within the reactor, assuming a uniform hydrogen distribution. A future step will involve incorporating spatial variations into the model to better represent the mass transfer phenomena occurring within the reactor. Implementing such a model would allow for a more detailed assessment of the thermal response of the hydride bed and the optimization of operational strategies.

Additionally, the modelling approach has been limited to the absorption phase, while the desorption process has not been considered. Since hydrogen storage systems operate in cyclic absorption-desorption modes, an important future development will be to extend the model to describe the desorption phase, considering the effects of heat supply, reaction kinetics, and equilibrium constraints. Including both absorption and desorption will allow a more complete evaluation of the storage system's efficiency and its thermal performance during continuous operation.

A promising direction for future research involves exploring the integration of multiple reactors operating in parallel. Studying the interaction between multiple reactors and their thermal coupling would provide valuable insights into the scalability of the technology for larger applications.

The model developed serves as a valuable tool for reactor design. Through a multidisciplinary approach that combines advanced modelling, material optimization, and improved system design, hydrogen storage using metal hydrides can become an increasingly viable and competitive solution in the energy transition landscape.

References

[1]   R. Neshovski, 'Home', United Nations Sustainable Development. [Online]. Available: https://www.un.org/sustainabledevelopment/

[2]   'THE 17 GOALS | Sustainable Development'. [Online]. Available: https://sdgs.un.org/goals

[3]   'Energy system', IEA. [Online]. Available: https://www.iea.org/energy-system

[4]   UNO, 'Obiettivo 7: Assicurare a tutti l'accesso a sistemi di energia economici, affidabili, sostenibili e moderni', ONU Italia. [Online]. Available: https://unric.org/it/obiettivo-7-assicurare-a-tutti-laccesso-a-sistemi-di-energia-economici-affidabili-sostenibili-e-moderni/

[5]   UNO, 'Obiettivo 13: Promuovere azioni, a tutti i livelli, per combattere il cambiamento climatico', ONU Italia. [Online]. Available: https://unric.org/it/obiettivo-13-promuovere-azioni-a-tutti-i-livelli-per-combattere-il-cambiamento-climatico/

[6]   'The European Green Deal: A growth strategy that protects the climate'. [Online]. Available: https://ec.europa.eu/stories/european-green-deal

[7]   'Fit for 55', Consilium. [Online]. Available: https://www.consilium.europa.eu/en/policies/fit-for-55/

[8]   'In evidenza: idrogeno - guidare la rivoluzione verde - Commissione europea'. [Online]. Available: https://commission.europa.eu/news/focus-hydrogen-driving-green-revolution-2021-04-14_it

[9]   'Fit for 55: shifting from fossil gas to renewable and low-carbon gases', Consilium. [Online]. Available: https://www.consilium.europa.eu/en/infographics/fit-for-55-hydrogen-and-decarbonised-gas-market-package-explained/

[10]   'Hydrogen and decarbonised gas market'. [Online]. Available: https://energy.ec.europa.eu/topics/markets-and-consumers/hydrogen-and-decarbonised-gas-market_en

[11]   'Fit for 55: towards more sustainable transport', Consilium. [Online]. Available: https://www.consilium.europa.eu/en/infographics/fit-for-55-afir-alternative-fuels-infrastructure-regulation/

[12]   M. Lototskyy, I. Tolj, Y. Klochko, M. W. Davids, D. Swanepoel, and V. Linkov, 'Metal hydride hydrogen storage tank for fuel cell utility vehicles', *Int. J. Hydrog. Energy*, vol. 45, no. 14, pp. 7958–7967, Mar. 2020, doi: 10.1016/j.ijhydene.2019.04.124.

[13]   'Supply – Electricity 2025 – Analysis', IEA. [Online]. Available: https://www.iea.org/reports/electricity-2025/supply

[14]   G. Sdanghi, G. Maranzana, A. Celzard, and V. Fierro, 'Review of the current technologies and performances of hydrogen compression for stationary and automotive applications', *Renew. Sustain. Energy Rev.*, vol. 102, pp. 150–170, Mar. 2019, doi: 10.1016/j.rser.2018.11.028.

[15]   'Hydrogen', Energy.gov. [Online]. Available: https://www.energy.gov/topics/hydrogen

[16]   P. Modi and K.-F. Aguey-Zinsou, 'Room Temperature Metal Hydrides for Stationary and Heat Storage Applications: A Review', *Front. Energy Res.*, vol. 9, p. 616115, Apr. 2021, doi: 10.3389/fenrg.2021.616115.

[17]   'DOE Technical Targets for Onboard Hydrogen Storage for Light-Duty Vehicles', Energy.gov. [Online]. Available: https://www.energy.gov/eere/fuelcells/doe-technical-targets-onboard-hydrogen-storage-light-duty-vehicles

[18]   G. Sdanghi *et al.*, 'A 70 MPa hydrogen thermally driven compressor based on cyclic adsorption-desorption on activated carbon', *Carbon*, vol. 161, pp. 466–478, May 2020, doi: 10.1016/j.carbon.2020.01.099.

[19] S. M. Aceves *et al.*, 'High-density automotive hydrogen storage with cryogenic capable pressure vessels', *Int. J. Hydrog. Energy*, vol. 35, no. 3, pp. 1219–1226, Feb. 2010, doi: 10.1016/j.ijhydene.2009.11.069.

[20] R. Paggiaro, P. Bénard, and W. Polifke, 'Cryo-adsorptive hydrogen storage on activated carbon. I: Thermodynamic analysis of adsorption vessels and comparison with liquid and compressed gas hydrogen storage', *Int. J. Hydrog. Energy*, vol. 35, no. 2, pp. 638–647, Jan. 2010, doi: 10.1016/j.ijhydene.2009.10.108.

[21] A. Züttel, 'Materials for hydrogen storage', *Mater. Today*, vol. 6, no. 9, pp. 24–33, Sep. 2003, doi: 10.1016/S1369-7021(03)00922-2.

[22] N. Klopčič, I. Grimmer, F. Winkler, M. Sartory, and A. Trattner, 'A review on metal hydride materials for hydrogen storage', *J. Energy Storage*, vol. 72, p. 108456, Nov. 2023, doi: 10.1016/j.est.2023.108456.

[23] J. Bellosta von Colbe *et al.*, 'Application of hydrides in hydrogen storage and compression: Achievements, outlook and perspectives', *Int. J. Hydrog. Energy*, vol. 44, no. 15, pp. 7780–7808, Mar. 2019, doi: 10.1016/j.ijhydene.2019.01.104.

[24] G. Sandrock, 'A panoramic overview of hydrogen storage alloys from a gas reaction point of view', *J. Alloys Compd.*, vol. 293–295, pp. 877–888, Dec. 1999, doi: 10.1016/S0925-8388(99)00384-9.

[25] S. S. Mohammadshahi, E. MacA. Gray, and C. J. Webb, 'A review of mathematical modelling of metal-hydride systems for hydrogen storage applications', *Int. J. Hydrog. Energy*, vol. 41, no. 5, pp. 3470–3484, Feb. 2016, doi: 10.1016/j.ijhydene.2015.12.079.

[26] D. P. Broom, *Hydrogen Storage Materials: The Characterisation of Their Storage Properties*. in Green Energy and Technology. London: Springer London, 2011. doi: 10.1007/978-0-85729-221-6.

[27] E. M. Dematteis, D. M. Dreistadt, G. Capurso, J. Jepsen, F. Cuevas, and M. Latroche, 'Fundamental hydrogen storage properties of TiFe-alloy with partial substitution of Fe by Ti and Mn', *J. Alloys Compd.*, vol. 874, p. 159925, Sep. 2021, doi: 10.1016/j.jallcom.2021.159925.

[28] R. Hancke, T. Holm, and Ø. Ulleberg, 'The case for high-pressure PEM water electrolysis', *Energy Convers. Manag.*, vol. 261, p. 115642, Jun. 2022, doi: 10.1016/j.enconman.2022.115642.

[29] N. Ahmadi, A. Dadvand, S. Rezazadeh, and I. Mirzaee, 'Analysis of the operating pressure and GDL geometrical configuration effect on PEM fuel cell performance', *J. Braz. Soc. Mech. Sci. Eng.*, vol. 38, no. 8, pp. 2311–2325, Dec. 2016, doi: 10.1007/s40430-016-0548-0.

[30] S. S. Mohammadshahi, T. Gould, E. MacA. Gray, and C. J. Webb, 'An improved model for metal-hydrogen storage tanks – Part 1: Model development', *Int. J. Hydrog. Energy*, vol. 41, no. 5, pp. 3537–3550, Feb. 2016, doi: 10.1016/j.ijhydene.2015.12.050.

[31] B. Satya Sekhar, M. Lototskyy, A. Kolesnikov, M. L. Moropeng, B. P. Tarasov, and B. G. Pollet, 'Performance analysis of cylindrical metal hydride beds with various heat exchange options', *J. Alloys Compd.*, vol. 645, pp. S89–S95, Oct. 2015, doi: 10.1016/j.jallcom.2014.12.272.

[32] U. Mayer, M. Groll, and W. Supper, 'Heat and mass transfer in metal hydride reaction beds: Experimental and theoretical results', *J. Common Met.*, vol. 131, no. 1–2, pp. 235–244, Mar. 1987, doi: 10.1016/0022-5088(87)90523-6.

[33] S. Suda, N. Kobayashi, and K. Yoshida, 'Reaction kinetics of metal hydrides and their mixtures', *J. Common Met.*, vol. 73, no. 1, pp. 119–126, Sep. 1980, doi: 10.1016/0022-5088(80)90350-1.

[34] F. S. Yang, G. X. Wang, Z. X. Zhang, X. Y. Meng, and V. Rudolph, 'Design of the metal hydride reactors – A review on the key technical issues', *Int. J. Hydrog. Energy*, vol. 35, no. 8, pp. 3832–3840, Apr. 2010, doi: 10.1016/j.ijhydene.2010.01.053.

[35] S. Nasrallah, 'Heat and mass transfer models in metal-hydrogen reactor', *Int. J. Hydrog. Energy*, vol. 22, no. 1, pp. 67–76, Jan. 1997, doi: 10.1016/S0360-3199(96)00039-0.

[36] N. O. of D. and Informatics, 'NIST Chemistry WebBook'. [Online]. Available: https://webbook.nist.gov/chemistry/